ADVANCES IN ELECTRONICS AND ELECTRON PHYSICS, VOL. 67

Open-Circuit Voltage Decay in Solar Cells

V. K. TEWARY*

Birla Institute of Technology and Science
Pilani-333031, India

S. C. JAIN†

Solid State Physics Laboratory
Delhi-110007, India

I. INTRODUCTION

Starting from the classic paper of Gossick (1955), open-circuit voltage decay (OCVD) has been a popular technique for measurement of excess carrier lifetime in p–n-junction diodes. In this technique, first a diode is forward biased for a long enough duration so that it attains a steady state. The forward current is then switched off. Keeping the diode in open circuit, the voltage decay is observed on a CRO. The decay curve in most cases contains a linear region. The slope of this region is, as shown by Gossick (1955), $(kT/q)(1/\tau_b)$ (for notations, see Appendix) from which τ_b can be determined.

The physical principle of OCVD can be understood as follows. The effect of a forward current in a diode is to inject excess carriers. The excess carrier concentration (ECC) at any point is determined by the balance of the following contributions (1) excess carrier generation, (2) recombination of carriers, and (3) diffusive motion of carriers. For the moment we neglect the contributions of drift field and the end surfaces of the diode. In steady state the space distribution of ECC, i.e., the excess carrier profile (ECP) does not change with time.

When the injection of excess carriers is switched off, the ECC at each point will decay to zero. Eventually the carrier concentration would assume its thermal equilibrium value. Initially, when the decay starts, the ECC as a function of time is determined by the diffusive motion of the carriers and their

* Present address: Institute for Materials Science and Engineering, United States Department of Commerce, National Bureau of Standards, Gaithersburg, Maryland 20899.

† Present address: Department of Electrical and Computer Engineering, University of Arizona, Tucson, Arizona 85721.

recombination. The diffusive motion depends upon the ECC gradient and therefore on the steady-state ECP. After a while the ECP will even out and the diffusive motion becomes negligible. Then the carriers decay by recombination only. The recombination rate is equal to ECC/τ_b (see, for example, Shockley, 1950). Thus ECC can be shown to have exponental dependence on time, viz. $\exp(-t/\tau_b)$. The junction voltage according to the Shockley relation is proportional to log of ECC at the junction. Hence the voltage will decay linearly with time and the slope of the linear region will be proportional to $1/\tau_b$. Obviously, in this region, the decay rate will be independent of the starting ECP, which mainly determines the diffusive motion of carriers.

A p–n junction solar cell is also a diode. In a solar cell the excess carriers can be injected electrically by a forward current or optically by illuminating it. The ECP in the steady state will obviously be different in the two cases (see, for example, McKelvey, 1966). The decay will start when the injection is stopped by switching off the forward current or the illumination as the case may be. From what has been described in the preceeding paragraph, initially the diffusive contribution will be significant, which depends upon the shape of the ECP. The initial shape of the decay curve will therefore depend upon whether the excess carriers were generated electrically or optically. The later part of the curve which signifies decay mainly by recombination will be independent of the manner in which excess carriers were injected in the steady state. Thus OCVD can also be induced optically in a solar cell from which τ_b can be measured.

The excess carriers' lifetime τ_b is an important material parameter of a solar cell. It determines the energy conversion efficiency of solar cells. This explains the strong topical interest in the OCVD technique. In addition, the OCVD technique is used in studying the switching behavior of diodes and solar cells and design of electronic pulse circuits, charge storage devices, and varactor diodes for frequency multiplication.

In this article our interest will be confined to theory of OCVD technique for determination of excess carrier lifetime in p–n-junction single-crystal solar cells. We shall discuss OCVD obtained by electrical as well as optical injection of excess carriers. The former will be referred to as forward-current-induced voltage decay (FCVD) and the latter as photovoltage decay (PVD). Henceforth, OCVD will refer jointly to FCVD and PVD. Obviously in an ordinary diode only FCVD is possible whereas both FCVD and PVD can be observed in solar cells.

In the present article we shall use the general word "device" to refer only to diodes and solar cells and no other devices. Although our main interest is in solar cells, we shall discuss some recent work on FCVD in diodes in so far as it is relevant to determination of τ_b in solar cells. Several review articles and monographs on FCVD in diodes are already available in the literature (see, for

example, Nosov, 1969). A glance at the table of contents will indicate the scope of the present article.

A. Structure of a Solar Cell

A solar cell has a diffused layer of p type or n type on top of a n- or p-type (respectively) base. Light enters from the top of the solar cell, through the diffused layer to the base (see Fig. 1). The excess carriers (both p and n type) are created throughout the solar cell in the diffused layer as well as the base. The diffused layer is also called an emitter. There is a space-charge layer between the emitter and the base. However, in this article, we have neglected the effect of the space-charge layer and assumed that the solar cell has a planar abrupt p–n junction. (see Section II.A).

The top of the emitter, viz. the front surface of the solar cell, has a grid electrical contact to allow light to enter the solar cell. The back surface of the base has a full ohmic contact. Modern solar cells also have a low–high junction (n–p–p^+ or p–n–n^+) in the base which gives the so-called back surface field (BSF). In such cases the base of the solar may be taken to extend from the p–n junction to the low–high junction.

The structure of an ordinary diode is similar to a solar cell except that there is no need for a grid contact at the top of the emitter. Usually both the front and the back surface of a diode have full ohmic contact.

Usually, the emitter in a modern device is heavily doped. The doping concentration may be of the order of $10^{17}\ \text{cm}^{-3}$–$10^{19}\ \text{cm}^{-3}$. The base, on the other hand is lightly doped, the doping concentration being about $10^{15}\ \text{cm}^{-3}$–$10^{16}\ \text{cm}^{-3}$.

In a forward-biased diode or an illuminated solar cell in steady state, excess carriers are stored in the emitter, the space-charge layer, and the base. When the steady state is interrupted by switching off the forward bias or the illumination, the excess carriers in all the three regions of the device emitter,

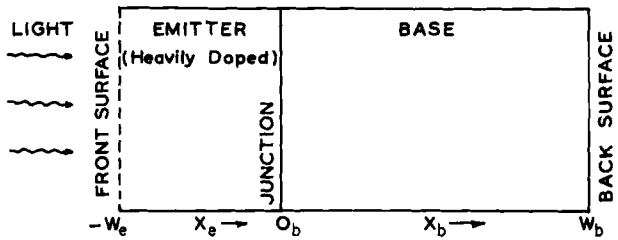

FIG. 1. Model of the p–n-junction solar cell or diode. A diode has an ohmic contact at the front surface, whereas a solar cell usually has a grid contact to allow for the light to enter.

space-charge layer, and base will decay. The effect of the space-charge layer is usually negligible except at low voltages (Sah *et al.*, 1957). In a typical modern silicon diode or solar cell the effect of the space-charge layer is negligible unless the junction voltage is lower than 0.4 V. In this article we shall not be interested in such low levels of injection. We shall therefore not discuss the effect of the space-charge layer. Unless otherwise obvious by context, in this article when we refer to low levels of injection it would mean that the level of injection is low enough for high injection effects to be neglected but not low enough for space charge effects to be significant.

Because of high doping in the emitter, the saturation current of the emitter is expected to be much less than that of the base. In such cases the injection efficiency of the emitter is close to unity and the characteristics of the device are determined from the base alone. Such devices are called base-dominated devices (solar cell or diodes). However, it has been found that the heavy nonuniform doping in the emitter causes band-gap narrowing which increases the saturation current of the emitter. The saturation current is further increased because carrier lifetime in the emitter is reduced due to processes like Auger recombination. Consequently, the effect of emitter cannot be ignored. In such cases OCVD becomes quite sensitive to the coupling of the ECP in the emitter and the base. This so-called p–n coupling is discussed in Sections IV and V at low injections and in Section VI at high injections.

B. Experimental Technique

The main objective of this article is to review theory of OCVD in solar cells and application of this theory to interpretation of experimental data with a view to determine τ_b. However, in order to give an idea of the nature of the OCVD experiments, a brief description of the experimental technique is given below. For details, reference may be made to the original papers quoted in the text (also see Nosov, 1969, for FCVD).

The schematic circuit diagrams for FCVD and PVD are shown in Figs. 2 and 3, respectively. In FCVD experiments, a pulse generator is used to provide

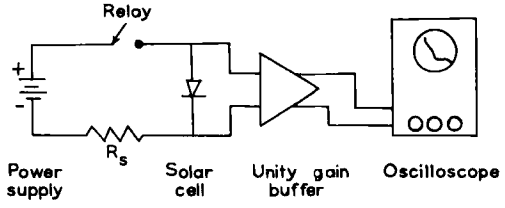

FIG. 2. Schematic circuit diagram for the forward-current-induced voltage decay in a diode/solar cell.

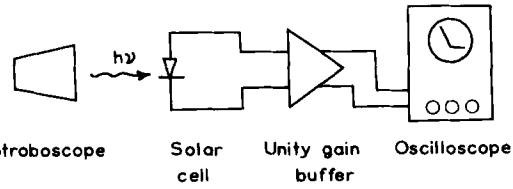

FIG. 3. Schematic circuit diagram for photovoltage decay in a solar cell.

a rectangular pulse. The length of the pulse should be long enough so that the device attains a steady state of foreward bias before the injection is switched off. In PVD, the light pulses can be generated by electronic stroboscopes or lasers. Both FCVD and PVD patterns are monitored on a CRO. In the FCVD experiments using lasers which give a single pulse, PVD pattern has to be observed on a storage oscilloscope.

II. BASIC FORMULATION

In this section we shall describe the model of a p–n-junction device on which the subsequent discussion is based. We shall also quote the ambipolar diffusion equation and steady-state solutions in some specific cases which will be used in the calculation of OCVD in later sections. Excellant reviews and monographs are available in the literature in which the steady-state characteristics of diodes and solar cells have been described in detail (see, for example, Moll, 1964; Shockley, 1950; McKelvey, 1966; Sze, 1981; Hovel, 1975; Neville, 1980; Fahrenbuch and Bube, 1983).

A. Model of a p–n-Junction Device

We consider a planar abrupt junction model of a p–n-junction device as shown in Fig. 1. In this model the space-charge effects are neglected. The space-charge effects are relatively insignificant except at low levels of injection (see, for example, Shockley, 1950). We shall also assume that the quasi-neutrality approximation (Shockley, 1950) is valid. According to this approximation the excess carrier concentrations of the two types, viz. n and p, are exactly equal everywhere and at all times. This is a useful and certainly conventional approximation, though not rigorously valid (see, for example, Shockley, 1950: McKelvey, 1966).

We further assume that the injection is uniform on any plane parallel to the junction. We thus treat the device as essentially a one-dimensional structure as

shown in Fig. 1. This figure also shows the coordinate axes. The origin is taken at the junction. The x axis is taken to be normal to the junction. The front surface is at $x = -d_e$ whereas the back surface is at $x = d_b$. The subscripts e and b refer to the emitter and the base, respectively. We shall model the two end surfaces by defining a surface recombination velocity (SRV). An ohmic contact will be represented by SRV $= \infty$.

The effect of BSF at the low–high junction can be modelled by defining an effective SRV at that back surface of the base, i.e., the low–high junction. In the ideal case the SRV at this junction can be assumed to be zero. We shall refer to such a device as an ideal BSF device in which SRV at the back surface of the base will be taken to the zero. A device with an ohmic contact at the back surface of the base (SRV $= \infty$) will be referred to as a conventional device.

In some cases d_e/L_e and d_b/L_b are much larger than unity. In such cases the thickness of the emitter and the base may be assumed to be infinite. Such a diode will be referred to as a thick diode. It may be remarked that in a solar cell, even if $d_e/L_e \gg 1$, it is not possible to approximate the thickness of the emitter to infinity. This is because the absorption of light in the solar cell is generally exponential and hence an infinitely thick emitter would imply that no light can reach the junction and the base. In a solar cell therefore, we shall always assume the emitter to have a finite thickness. The base, however, can be approximated to be infinitely thick if $d_b/L_b \gg 1$. Such a solar cell will be referred to as a "thick" solar cell.

B. Ambipolar Diffusion Equation

In this section we shall present the ambipolar diffusion equation for excess carriers. The ambipolar equation is derived by combining the diffusion equation for the two types of carriers and using the quasi-neutrality approximation. The ambipolar equation does not refer to either of the two types of carriers in isolation but refers to both.

For the model described in the preceeding section, the ambipolar equation in the emitter is as follows:

$$D_e^* \frac{\partial^2 q_e}{\partial x^2} - \mu_e^* E_e \frac{\partial q_e}{\partial x} + g_e^* - \frac{q_e}{\tau_e^*} = \frac{\partial q_e}{\partial t} \tag{1}$$

where

$$D_e^* = \frac{(q_{e0} + q_{em} + 2q_e) D_e D_{em}}{(q_{e0} + q_e) D_e + (q_{em} + q_e) D_{em}} \tag{2}$$

$$\mu_e^* = \frac{(q_{em} - q_{e0}) \mu_e \mu_{em}}{(q_{e0} + q_e) \mu_e + (q_{em} + q_e) \mu_{em}} \tag{3}$$

and the excess carrier lifetime τ_e^* is defined by

$$\frac{q_e}{\tau_e^*} = \frac{q_{e0} + q_e}{\tau_e} - \frac{q_{e0}}{\tau_{e0}} = \frac{q_{em} + q_e}{\tau_{em}} - \frac{q_e}{\tau_{em0}} \tag{4}$$

The ambipolar equation for the base is similar to Eq. (1) with the subscript e replaced by b. The ambipolar equation is a nonlinear equation. However, as we shall see below, it becomes a linear equation in the low and high injection limits.

1. Low Injection Limit

In this limit $q_e \ll q_{em}$. For a strongly extrinsic semiconductor, $q_{e0} \ll q_{em}$. In this case, we obtain from Eqs. (2) and (3)

$$D_e^* = D_e \tag{5}$$

and

$$\mu_e^* = \mu_e \tag{6}$$

Further, in the low injection approximation τ_e is nearly equal to τ_{e0} and therefore, from Eq. (4)

$$\tau_e^* = \tau_e \tag{7}$$

Thus we see that, in the low injection approximation in a strongly extrinsic semiconductor, the ambipolar diffusion equation reduces to the linear diffusion equation for the minority carriers.

2. High Injection Limit

The high injection effects become significant when the excess carrier concentration becomes comparable to the thermal equilibrium value of the majority carrier concentration. The high injection limit is defined by $q_e \gg q_{em}$. In this limit, Eqs. (2) and (3) reduce to the following

$$D_e^* = \frac{2D_eD_m}{D_e + D_m} \tag{8}$$

and

$$\mu_e^* = 0 \tag{9}$$

The excess carrier lifetime τ_e^* has a rather complicated dependence on the level of injection (see, for example, Baliga, 1981). Moreover, at high injections certain other processes such as the Auger process make significant contributions to the excess carrier lifetime (see, for example, Gandhi, 1977). We shall not discuss the dependence of τ_e^* on q_e in this article. We only define $\tau_{e\infty}$

as the high injection limit of τ_e^* so that in this limit

$$\tau_e^* = \tau_{e\infty} \tag{10}$$

From Eqs. (8) and (9) we see that the ambipolar quantities reduce to their values for intrinsic semiconductors (i.e., for $q_{e0} = q_{em}$) in the high injection limit. This is of course physically expected because when the excess carrier concentration is much larger than the doping concentration of the semiconductor, the physical quantities cannot be sensitive to the nature and the level of doping. The semiconductor will therefore behave as an undoped, i.e., an intrinsic semiconductor. It may also be noted that in the high injection limit, Eq. (1) becomes a linear diffusion equation again.

C. Boundary Conditions

The ambipolar equation, i.e., Eq. (1) is a second-order differential equation which gives the excess carrier profile, i.e., $q_e(x, t)$ in the emitter. A similar equation would give the excess carrier profile $q_b(x, t)$ in the base. However, in order to specify the solution, i.e., the ECPs, we have to prescribe certain boundary conditions. These boundary conditions may specify the boundary value of the function (Dirichlet type) or its derivative (Neumann type) or their combination.

In the present abrupt junction model as shown in Fig. 1, the space-charge layer has been neglected. The ECPs $q_e(x, t)$ and $q_b(x, t)$ are therefore directly coupled at the junction $x = 0$. The coupling, as we shall see below, arises from the boundary conditions.

In order to fix our ideas, first we consider the steady state. However, the boundary conditions discussed below, in general, will also apply to transient state. In the steady state, by definition, the time derivative of q_e i.e., the right-hand side of equation (1) is zero. The total number of boundary conditions required in the steady state is obviously four; two for $q_e(x)$ in the emitter and two for $q_b(x)$ in the base. We can specify one boundary condition at the front surface $x = -d_e$, one at the back surface $x = d_b$, and two at the junction $x = 0$. These are described below.

1. Boundary Condition at the Front Surface ($x = -d_e$)

$$dq_e/dx = S_e q_e - \eta N_0 \tag{11}$$

This boundary condition was derived by Tewary and Jain (1980). The second term on the right-hand side of Eq. (11) accounts for generation of carriers at the front surface. This term contributes only in the case of an illuminated solar cell. In case of electrical injection of carriers in a diode or a

solar cell with no incident light, $N_0 = 0$. In this case, as well as when $\eta = 0$, Eq. (11) reduces to the conventional boundary condition (see, for example, Shockley, 1950; McKelvey, 1966; Sze, 1981).

In case of an ohmic contact as in a diode, $S_e = \infty$ and Eq. (11) reduces to

$$q_e(-d_e) = 0 \qquad \text{(ohmic contact)} \tag{12}$$

2. Boundary Condition at the Back Surface ($x = d_b$)

$$dq_b(d_b)/dx = -S_b q_b(d_b) \tag{13}$$

The generation of carriers at the back surface, i.e., the term corresponding to the second term in Eq. (11) can be neglected in this case. For a conventional solar cell or a diode with no BSF and an ohmic contact at the base, $S_b = \infty$. In this case, as in Eq. (12),

$$q_b(d_b) = 0 \qquad \text{(conventional device)} \tag{14}$$

In a solar cell or a diode containing BSF, the back surface is modeled by assigning an effective value to S_b. An ideal BSF device is defined by $S_b = 0$ so that in this case

$$dq_b(d_b)/dx = 0 \qquad \text{(ideal BSF device)} \tag{15}$$

3. Boundary Conditions at the p–n Junction ($x_e = x_b = 0$)

We need to specify two boundary conditions at the p–n junction. One of them called the current condition, relates the gradients of the excess carrier profiles at the junction to the total current through the junction. The other boundary condition is called the voltage condition and relates the heights of the excess carrier profiles at the junction to the voltage at the junction or the terminals of the device.

In practice, it is convenient to formally prescribe the following boundary conditions

$$q_e(x = 0) = q_{ej} \tag{16}$$

and

$$q_b(x = 0) = q_{bj} \tag{17}$$

Thus the solutions of the diffusion equations in the emitter and the base regions are specified, respectively, in terms of q_{ej} and q_{bj}. These quantities are then determined using the voltage condition which is given later in this section. The current voltage relation can then be determined by using the current condition which is given below.

4. Current Condition

The total current through the junction J_j is the sum of the emitter and the currents at the junction. Thus

$$J_j = J_{ej} - J_{bj} \tag{18}$$

where the appropriate signs of J_{ej} and J_{bj} are to be taken depending upon the type of the carriers (p or n). The emitter and the base currents at the junction are given by

$$J_{ej} = -D_e\left(\frac{dq_e}{dx}\right)_0 + \mu_e q_{ej} E_{ej} \tag{19}$$

and

$$J_{bj} = -D_b\left(\frac{dq_b}{dx}\right)_0 + \mu_b q_{bj} E_{bj} \tag{20}$$

where E_{ej} and E_{bj} denote the values of the drift field in the emitter and the base at the junction $x = 0$. The appropriate signs of μ_e and μ_b are to be chosen depending upon the type of carriers (p or n).

The current J_j is a measurable quantity and is determined from the experimental conditions. Thus Eq. (18) along with Eqs. (19) and (20) provide one of the boundary conditions at the junction. We shall be particularly interested in the open-circuit case, i.e., when $J_j = 0$. In this case the required boundary condition is given by

$$D_b\left(\frac{dq_b}{dx}\right)_0 - D_e\left(\frac{dq_e}{dx}\right)_0 - \mu_b q_{bj} E_{bj} + \mu_e q_{ej} E_{ej} = 0 \tag{21}$$

(open-circuit condition)

5. Voltage Condition

The voltage condition relates the excess carrier concentration at the junction on its either side (emitter and the base) to the voltage in the device. Here, one needs to distinguish between the voltage at the junction and the terminals of the device. The terminal and the junction voltage are, in general, different because of the voltage drops in the quasi-neutral regions of the device. This voltage drop arises primarily due to the ohmic resistance of the quasi-neutral regions when a current is flowing and the Dember effect which arises due to the difference in the mobilities of the two types of carriers. For a detailed discussion of these contribution, see, for example, McKelvey (1966).

There has been considerable confusion and controversy in the literature regarding the voltage condition to be used (see, for example, Hauser, 1971;

Heasell, 1979; Nussbaum, 1969, 1975, 1979; Guckell *et al.*, 1977; Scharfetter *et al.*, 1963; Van der Ziel, 1966; Van Vliet, 1966). We shall not attempt to resolve this controversy here but only report that it is now generally believed that the junction voltage is described by Fletcher conditions (Fletcher, 1957; see also Dhariwal *et al.*, 1976), whereas the terminal voltage is described by Misawa conditions (Misawa, 1956; Hauser, 1971). These are quoted below.

6. Fletcher Conditions

$$q_{ej} = \frac{q_{e0} + q_{b0}\exp\{q(V_j - V_D)/kT\}}{1 - \exp\{2q(V_j - V_D)/kT\}}[\exp(qV_j/kT) - 1] \tag{22}$$

$$q_{bj} = \frac{q_{b0} + q_{e0}\exp\{q(V_j - V_D)/kT\}}{1 - \exp\{2q(V_j - V_D)/kT\}}[\exp(qV_j/kT) - 1] \tag{23}$$

7. Misawa Conditions

These conditions are quite complicated in the case when a current is flowing through the device. However, in the open-circuit case and using the charge balance approximation, the Misawa conditions can be written in the following form:

$$q_{ej}^2 + q_{em}q_{ej} = q_{bj}^2 + q_{bm}q_{bj} = q_e^2[\exp(qV_a/kT) - 1] \tag{24}$$

In most cases of practical interest the unity in the square brackets in the extreme right of the above equation is negligible. We thus obtain

$$q_{ej} = [q_e^2\{\exp(qV_a/kT) - 1\} + q_{em}^2/4]^{1/2} - q_{em}/2 \tag{25}$$

and

$$q_{bj} = [q_e^2\{\exp(qV_a/kT) - 1\} + q_{bm}^2/4]^{1/2} - q_{bm}/2 \tag{26}$$

In the extreme high injection limit, the Misawa conditions reduce to the following simple form which has been used frequently in the literature

$$q_{ej} = q_{bj} = q_i\exp\{qV_a/2kT\} \qquad \text{(high injection limit)} \tag{27}$$

8. Low Injection Limit

Fortunately, in the limit of low injections, the situation is quite clear. Both Fletcher and Misawa conditions reduce to the well-known Shockley boundary condition as given below.

$$q_{ej} = q_{e0}[\exp(qV_j/kT) - 1] \tag{28}$$

and

$$q_{bj} = q_{b0}[\exp(qV_j/kT) - 1] \tag{29}$$

In the low injection limit the Dember voltage is negligible. The difference between the terminal and the junction voltage arises mainly due to the ohmic drop in the quasi-neutral regions so that

$$V_a = V_j \pm qJ_jR_s \tag{30}$$

In the open-circuit case $J_j = 0$ so that in the low injection limit

$$V_a = V_j \tag{31}$$

Even at fairly high injections, the Dember voltage is only a small percentage of V_j so that Eq. (31) may be taken as a reasonable approximation (McKelvey, 1966).

In the time-dependent case the boundary conditions given above at the two surfaces as well as at the junction have to be obeyed at all times. In addition, the excess carrier profiles $q_e(x, t)$ and $q_b(x, t)$ have to be specified for values of x at a certain instant of time. In latter sections, we shall be interested in transients starting at $t = 0$ when the steady state persisted until $t = 0$. We therefore prescribe initial conditions as follows:

$$q_e(x, t = 0) = q_{es}(x) \tag{32}$$

and

$$q_b(x, t = 0) = q_{bs}(x) \tag{33}$$

D. Solution of Steady-State Diffusion Equation in a Diode

In this section we shall briefly describe the solution of the linear diffusion equation for a diode in the steady state of electrical injection. In what follows we shall assume the drift field to be constant with respect to x. It implies that the doping profile is exponential. In practice doping profiles are rarely such. However, for practical purposes a constant drift field is a reasonable and certainly convenient approximation. In many devices the drift field can also be assumed to be zero.

We write the diffusion equations in the emitter and the base in terms of dimensionless variables X_e and X_b as follows:

Emitter ($-W_e \leq X_e \leq 0$):

$$\frac{d^2q_e}{dX_e^2} + 2F_e\frac{dq_e}{dX_e} - q_e = 0 \tag{34}$$

Base ($0 \leq X_b \leq W_b$):

$$\frac{d^2q_e}{dX_b^2} + 2F_b\frac{dq_b}{dX_b} - q_b = 0 \tag{35}$$

Equations (34) and (35) can be obtained from the ambipolar equations in the emitter and the base regions [for example, Eq. (1) for the emitter] by taking their low injection limits and transforming to the dimensionless variables X_e and X_b, respectively. In case of electrical injection in a diode, the excess carriers are injected at the junction. The generation terms g_e^* and g_b^* are taken to be zero everywhere. The injection of excess carriers at the junction is accounted for by using the voltage condition. The corresponding equations in the high injection limit will have the same form as Eqs. (34) and (35) but with redefined variables X_e and X_b and no drift field term.

We shall first give the solutions of Eqs. (34) and (35) for $F_e = F_b = 0$. The solutions for nonzero values of F_e and/or F_b can be obtained from these solutions by using a simple transformation which is given at the end of this section.

1. Thick Diodes ($W_{e,b} = \infty$)

Using the boundary conditions as given by Eqs. (12), (14), (16), and (17) we obtain

$$q_e(X_e) = q_{ej} \exp(X_e) \qquad (-\infty \leq X_e \leq 0) \tag{36}$$

and

$$q_b(X_b) = q_{bj} \exp(-X_b) \qquad (0 \leq X_b \leq \infty) \tag{37}$$

The current voltage (I–V) relation can be easily obtained by using Eqs. (18), (28), and (29) and is

$$J_j = [J_0 \exp(qV_j/kT) - 1] \tag{38}$$

where

$$J_0 = J_{e0} + J_{b0} \tag{39}$$

$$J_{e0} = D_e q_{e0}/L_{e0} \tag{40a}$$

and

$$J_{b0} = D_b q_{b0}/L_{b0} \tag{40b}$$

Equation (38) is the well-known Shockley relation for a diode. In fact, this relation is obeyed individually by the emitter and the base currents, which can be verified by using Eqs. (19), (20), (28), and (29) for zero-drift field which gives

$$J_{ej}/J_{e0} = J_{bj}/J_{b0} = \exp(qV_j/kT) - 1 \tag{41}$$

2. Thin Diodes ($W_{e,b}$ is finite)

a. Ohmic Contacts at Both Ends. In this case also the relevant boundary conditions are given by Eqs. (12), (14), (16), and (17). The solutions are as

follows:

$$q_e(X_e) = q_{ej}\frac{\sinh(X_e + W_e)}{\sinh W_e} \qquad (-W_e \le X_e \le 0) \tag{42}$$

$$q_b(X_b) = q_{bj}\frac{\sinh(W_b - X_b)}{\sinh W_b} \qquad (0 \le X_b \le W_b) \tag{43}$$

The I–V relation can be obtained by using Eqs. (18), (28), and (29) as in the preceeding case for thick diodes. It can be verified that the form of the I–V relation is the same as in Eq. (38). However, the expression for the saturation current is modified as follows:

$$J^*_{e0} = \frac{D_e q_{e0}}{L_{e0}} \coth W_e \tag{44}$$

and

$$J^*_{b0} = \frac{D_b q_{b0}}{L_{b0}} \coth W_b \tag{45}$$

Thus, the effect of finite thickness of the emitter and the base of a diode is to increase their saturation currents each by a factor equal to the hyperbolic cotangent of their thickness.

b. Ohmic Contact at the Front Surface and BSF in the Base. As described in Section II.C, we model the BSF in the base by defining an effective value of S_b. In this case the base is assumed to extend from the p–n junction to the low–high junction (i.e., p–p^+ junction in case of an n or p diode).

The relevant boundary conditions in this case are given by Eqs. (12), (13), (16), and (17). The solution in the emitter is same as given by Eq. (42). The solution in the base is ($0 \le X_b \le W_b$)

$$\frac{q_b(X_b)}{q_{bj}} = \frac{\cosh(W_b - X_b) + S^*_b \sinh(W_b - X_b)}{\cosh W_b + S^*_b \sinh W_b} \tag{46}$$

where the dimensionless SRV S^*_b is defined as

$$S^*_b = S_b \tau_b / L_b \tag{47}$$

In this case also the I–V relation has the same form as the Shockley relation given by Eq. (38). The effect of S^*_b is to further modify the base saturation current in Eq. (45). As mentioned earlier, for an ideal BSF diode $S_b = 0$, whereas for a conventional diode with an ohmic contact at the back $S_b = \infty$. In the latter case Eq. (46) reduces to Eq. (43).

3. Solution for a Constant Drift Field

We shall now indicate a method by which solution of the diffusion equation containing a constant drift field term can be obtained. Consider, for example, Eq. (35). We introduce the transformation

$$q_b(X_b) = y(X_b)\exp(-F_b X_b) \tag{48}$$

which reduces Eq. (35) to

$$\frac{d^2y}{dX_b^2} - y(1 + F_b^2) = 0 \tag{49}$$

This equation has the same form as the diffusion equation without a drift field. Its solution can be obtained as in Sections II.D.1 and II.D.2. The effect of the drift field is to modify the excess carrier profile by the exponential factor as given by Eq. (48) and the diffusion length L_b to an effective diffusion length L_b^* defined as follows:

$$1/L_b^* = (1 + F_b^2)^{1/2}/L_b \tag{50}$$

E. Solution of Steady-State Diffusion Equation for an Illuminated Solar Cell

As in Section II.D, we write the steady-state diffusion equations for the emitter and the base of an illuminated solar cell in terms of the dimensionless variables X_e and X_b as follows:

Emitter $(-W_e \leq X_e \leq 0)$:

$$\frac{d^2q_e}{dX_e^2} - q_e = g_e(X_e) \tag{51}$$

Base $(0 \leq X_b \leq W_b)$:

$$\frac{d^2q_b}{dX_b^2} - q_b = g_b(X_b) \tag{52}$$

where the dimensionless generation rates are defined as

$$g_e(X_e) = \tau_e g_e^*(X_e) \tag{53}$$

and

$$g_b(X_b) = \tau_b g_b^*(X_b) \tag{54}$$

For the generation rates, we take the usual exponential form as

$$g_e^*(X_e) = C_e(N_0/L_e)\exp[-C_e(X_e + W_e)] \tag{55}$$

and

$$g_b^*(X_b) = C_b(N_{0j}/L_b)\exp(-C_bX_b) \tag{56}$$

where N_0 and N_{0j} denote the number of photons incident per unit/time per unit area at the front surface (i.e., the emitter) and the junction, respectively. We have neglected the drift field which can be included by using the transformation defined by Eq. (48).

1. Thick Solar Cell ($W_b = \infty$)

First we consider a "thick" solar cell and take $W_b = \infty$. This case has been discussed by Sharma *et al.* (1981). They have derived the following expression for the excess carrier profile in the base using the boundary conditions as given by Eqs. (14) and (17).

$$q_{bs}(X_b) = Ke^{-X_b} - \frac{N}{C_b - 1}\exp(-C_bX_b) \qquad (0 \le X_b \le \infty) \tag{57}$$

where

$$K = q_{bj} + N/(C_b - 1) \tag{58}$$

and

$$N = \frac{C_bN_{0j}\tau_b}{L_b(1 + C_b)} \tag{59}$$

The junction potential is related to q_{bj} at low injections through the Shockley condition given by Eq. (29). The solution for the emitter can be easily obtained by using the boundary conditions given by Eqs. (11) and (16) and will not be quoted here. The total saturation current in this model can be shown to be

$$J_0 = J_{b0} + J_{e0}\frac{S_e^* \cosh W_e + \sinh W_e}{\cosh W_e + \sinh W_e} \tag{60}$$

The open-circuit voltage V_j is related to the light-generated current J_g through

$$V_j = (kT/q)\ln(1 + J_g/J_0) \tag{61}$$

The light-generated current J_g, which is equal in magnitude to the short circuit current in the solar cell, is proportional to the intensity of incident light and is

given by

$$J_g = J_{eg} + J_{bg} \tag{62}$$

where J_{eg} and J_{bg} denote, respectively, the contributions of the emitter and the base to J_g. The expression for J_{eg} is somewhat complicated (Sharma *et al.*, 1981) and is not needed here. It may be mentioned, however, that it is proportional to N_0. The expression for J_{bg} is

$$J_{bg} = C_b N_{0j}/(1 + C_b) \tag{63}$$

We shall obtain the excess carrier profile in the specific case of a base-dominated solar cell in open-circuit configuration which will be useful in Section III.B. In a base-dominated solar cell the effect of the emitter, by definition is negligible. In this case the zero-current condition given by Eq. (21) requires only the derivative of $q_B(X_B)$ to be zero at $X_b = 0$. By applying this condition, Eq. (57) gives

$$q_{bs}(X_b) = \frac{N}{C_b - 1}[C_b e^{-X_b} - e^{-C_b X_b}] \tag{64}$$

It can be easily verified that in this case N, as defined by Eq. (59), is equal to q_{bj}.

2. Thin Solar Cell (W_b is finite)

We now consider a solar cell in which the base thickness W_b is finite. We shall assume that the effect of the emitter is negligible so that the solar cell is a base-dominated solar cell. It may have an ohmic contact at the back or a BSF which, as in Section II.D.2, will be modeled by assigning an effective value to the SRV at the back surface.

We shall give below the excess carriers profiles in the base for two limiting cases—one for $S_b = \infty$ corresponding to an ohmic contact at the base and the other for $S_b = 0$, which is referred as an ideal BSF cell. For the more general case of finite S_b and a constant drift field in the base, see Sharma and Tewary (1982), Kennedy (1962), and Wolf (1963).

a. Conventional Solar Cell ($S_b = \infty$). The relevant boundary conditions in this case are given by Eqs. (14) and (17). The solution of the diffusion equation for the base region is then given by

$$q_b(X_b)/q_{bj} = D_1/D_2 \tag{65}$$

where

$$D_1 = \exp(-C_b X_b) + C_b \exp(X_b) - D_3[\exp(X_b) + \exp(-X_b)] \tag{66}$$

$$D_2 = 1 + C_b - 2D_3 \tag{67}$$

and

$$D_3 = \frac{C_b \exp(W_b) + \exp(-C_b W_b)}{\exp(W_b) + \exp(-W_b)} \tag{68}$$

b. Ideal BSF Solar Cell ($S_b = 0$). In this case the relevant boundary conditions are given by Eqs. (15) and (17). The required solution is as follows

$$\frac{q_b(X_b)}{q_{bj}} = D_4/D_5 \tag{69}$$

where

$$D_4 = \exp(-C_b X_b) + C_b \exp(X_b) + C_b D_b[\exp(X_b) + \exp(-X_b)] \tag{70}$$

$$D_5 = 1 + C_b + 2C_b D_b \tag{71}$$

and

$$D_6 = \frac{\exp(-C_b W_b) - \exp(W_b)}{\exp(W_b) - \exp(-W_b)} \tag{72}$$

III. OCVD in Base-Dominated Devices

In this section we shall discuss OCVD in base-dominated devices, i.e., solar cells and diodes in which the effect of the emitter is negligible and the decay characteristics are determinated by the base alone. Both FCVD and PVD will be discussed. For PVD we shall consider the case of a long as well as a short pulse. Some experimental results on PVD will also be discussed. The high injection effects will not be considered in this section.

A. FCVD in Diodes

We consider a forward biased diode in steady state. As given by Eq. (30) the terminal potential is related to the junction potential as follows:

$$V_{a0} = V_{j0} + I_F R_s \tag{73}$$

where the subscript zero on V_a and V_j denotes their steady-state values and I_F is the forward current.

We now assume that the forward current is instantaneously switched off at time $t = 0$. Now the diode is in open-circuit configuration while the voltage

across the diode will decay to zero. The ohmic part of the terminal voltage will decay instantaneously. Hence the terminal voltage which is the one measured experimentally, will show an instantaneous drop. This voltage drop will be equal to the ohmic contribution to V_{a0} and is given by

$$\Delta V_0 = \Delta V_s = I_F R_s \tag{74}$$

This part of the voltage decay curve will appear as a vertical line at $t = 0$ on the CRO screen and can be easily measured. Since I_F is known from the steady-state measurements, R_s can be determined from the measured value of ΔV_s (see, however, Section IV).

Our main interest lies in the decay of V_j, which is the remaining part of V_a after separating out the ohmic contribution. Since the diode is open circuited after $t = 0$, Eq. (31) will be valid. The decay of V_j is determined by the decay of q_{bj} in accordance with Eq. (29). The time dependence of q_{bj} can be calculated theoretically by solving the ambipolar diffusion equation for the base [see Eq. (1)]. In the low injection limit in which we are presently interested, the ambipolar equation reduces to the diffusion equation for minority carriers (see Section II.B.1). This equation written in terms of the dimensionless variables is (for $z > 0$) ($0 \leq X \leq \infty$)

$$\frac{\partial^2 q_b(X,z)}{\partial X^2} + 2F_b \frac{\partial q_b(X,z)}{\partial X} - q_b(X,z) = \frac{\partial q_b(X,z)}{\partial z} \tag{75}$$

where $X = x/L_b$ and $z = t/\tau_b$. The subscript b has been dropped from X for notational brevity. In this section we shall assume $F_b = 0$, i.e., there is no drift field.

In the steady state the right-hand side of Eq. (75) is zero and this equation reduces to Eq. (34) for zero-drift field. The transient starts at $z = 0$ when the forward bias is switched off. Equation (75) has to be solved, therefore, after $z = 0$. The boundary conditions are prescribed as given by Eqs. (14) and (17) and the initial condition as given by Eq. (33) where the initial steady-state profile is given by Eq. (37).

After the forward bias is switched off, i.e., for $z > 0$, the diode is in open circuit. We have to therefore also impose the zero-current condition as given by Eq. (21). This equation, in the present approximation of zero-drift field and no emitter contribution, reduces to the following

$$\left[\frac{\partial q_b(X,z)}{\partial X}\right]_{X=0} = 0 \tag{76}$$

The solution of Eq. (75) subject to the above boundary and initial conditions can be obtained easily (see, for example, Nosov, 1969) and is

as ($z > 0, 0 \leq X \leq \infty$)

$$\frac{q_b(X,z)}{q_{bj}(0)} = \frac{1}{2}\left[e^{-X}\operatorname{erfc}\left(\sqrt{z} - \frac{X}{2\sqrt{z}}\right) + e^{X}\operatorname{erfc}\left(\sqrt{z} + \frac{X}{2\sqrt{z}}\right)\right] \tag{77}$$

With the help of Eq. (29), we obtain the following expression for voltage decay from Eq. (75):

$$\frac{\exp[V_1(z)] - 1}{\exp[V_1(0)] - 1} = \operatorname{erfc}\sqrt{z} \tag{78}$$

where

$$V_1(z) = qV_j(z)/kT$$

As long as the following inequality is satisfied

$$\exp[V_1(z)] \gg 1 \tag{79}$$

Eq. (78) can be written in the following simple form:

$$\Delta V_1(z) \equiv V_1(z) - V_1(0) = \ln[\operatorname{erfc}\sqrt{z}] \tag{80}$$

Equation (80) gives the well-known expression for FCVD that was first derived by Gossick (1955). For large z since $\operatorname{erfc}\sqrt{z}$ behaves like $\exp(-z)$, we see that

$$\Delta V_1(z) \approx -z \qquad (z \gg 1) \tag{81}$$

or

$$V_j(t) - V_j(0) = -(kT/q)(t/\tau_b) \tag{82}$$

We see from Eq. (82) that, for large t, the decaying voltage has a linear dependence on t. The slope of the linear region is $kT/q\tau_b$. Since the slope of the linear region can be easily measured the excess carrier lifetime can be determined with reasonable accuracy. As we have already seen from Eq. (74), the vertical drop at $t = 0$ in the FCVD curve gives R_s. Thus FCVD provides a convenient method for determining R_s as well as τ_b.

The main features of FCVD curve in a thick diode are

1. Vertical drop at $t = 0$ due to ohmic contribution
2. Some curvature in the initial portion of the FCVD curve as predicated by Eq. (79) for low values of z
3. A linear region in the curve with slope unity [in $V_1(z)$ versus z curve]

For even larger z, the junction voltage becomes too small, the space-charge effects become significant, and the theory as given above is not valid. The

behavior of this part of the FCVD curve is quite complicated and is outside the scope of this article. It is also not of any interest as far as the determination of excess carrier lifetime is concerned.

B. PVD in Thick Solar Cells

In this section we shall discuss PVD in a thick solar cell, i.e., assuming that the thickness of the base is infinite. We shall consider only monochromatic illumination. We first consider PVD induced by a long pulse. In this case the solar cell is assumed to have been illuminated in the open-circuit configuration for a long enough duration so that it has reached a steady state. The illumination is switched off at $t = 0$ when the decay starts.

After $t = 0\,(z = 0)$, the excess carrier concentration is given by the solution of Eq. (75). As in Section III.A, we assume that $F_b = 0$. All the boundary and the initial conditions as prescribed in Section III.A are also valid in the present case except that the initial excess carrier profile is given by Eq. (64) and not Eq. (37). This case has been studied by Jain (1981), whose results will be reviewed here.

By using the Laplace transform method, Jain (1981) has obtained the following expression for the excess carrier profile for $z > 0$:

$$\frac{q_b(X,z)}{q_{bj}(0)} = \frac{e^{-z}}{C-1}[Cf(X,z) - f(CX, C^2z)] \tag{83}$$

where, again for notational brevity, we have dropped the subscript b from X, z, and C, and

$$f(X,z) = e^z\left[e^{-X} - \frac{1}{2}e^{-X}\operatorname{erfc}\left(\frac{X}{2\sqrt{z}} - \sqrt{z}\right) + \frac{1}{2}e^{X}\operatorname{erfc}\left(\frac{X}{2\sqrt{z}} + \sqrt{z}\right)\right] \tag{84}$$

Equation (83) gives the following expression for the excess carrier concentration at the junction:

$$\frac{q_{bj}(z)}{q_{bj}(0)} = \frac{e^{-z}}{C-1}[CS(z) - S(C^2z)] \tag{85}$$

where

$$S(z) = e^z \operatorname{erfc}\sqrt{z} \tag{86}$$

By using the Shockley voltage condition given by Eq. (29), we obtain the following expression for PVD:

$$\Delta V_1(z) = -z + \ln\left[\frac{CS(z) - S(C^2 z)}{C - 1}\right] \tag{87}$$

For large z, the function $S(z)$ has the following asymptotic expansion (see, for example, Abramowitz and Stegun, 1965):

$$S(z) = \frac{1}{\sqrt{\pi z}}\left[1 - \frac{1}{2z} + \frac{1}{4z^2}\cdots\right] \tag{88}$$

Thus we see that for large z, $S(z)$ tends to unity and hence the contribution of the second term on the right-hand side of Eq. (87) vanishes. In this limit, as in the case of FCVD in diodes,

$$\Delta V_1(z) \approx -z \tag{89}$$

This equation shows that at large times, in principle, PVD curve also has a linear dependence on time with exactly the same slope as the FCVD curve from which τ_b can be determined. However, the location and the extent of the linear region will depend upon the value of C in Eq. (87). This is because, depending upon the value of C, the $S(z) = 1$ limit may not reach while the inequality (79) is still satisfied.

Figure 4 taken from Jain (1981) shows the dependence of $V_1(z)$ on z for different values of C as calculated from Eq. (87). This figure also gives FCVD curve as calculated from Eq. (80). We see from this figure that for larger values of C PVD curves come closer to the FCVD curve. Mathematically this behavior can be expected from Eq. (87) by noting that for $C \to \infty$

$$S(C^2 z) \ll S(z) \tag{90}$$

and in this limit Eq. (85) becomes identical to Eq. (80). This could also be anticipated from the steady-state excess carrier profile for an illuminated solar cell as given by Eq. (64). It may be verified that in the limit $C \to \infty$, Eq. (64) becomes identical to Eq. (37) which gives the excess carrier profile in a forward-biased diode. In general, the difference between PVD and FCVD arises only from the difference between their initial excess carrier profiles in the steady state.

Physically the similarity between FCVD and PVD for large values of C can be understood as follows. A large C, i.e., a large α implies a smaller absorption length (the range in which most of the photons are absorbed). In the limit when the absorption length is $0\,(C \to \infty)$, all the light will be absorbed within an infinitesimal range close to the junction. In this limit, there will be no generation of excess carriers anywhere in the base of the solar cell except at the

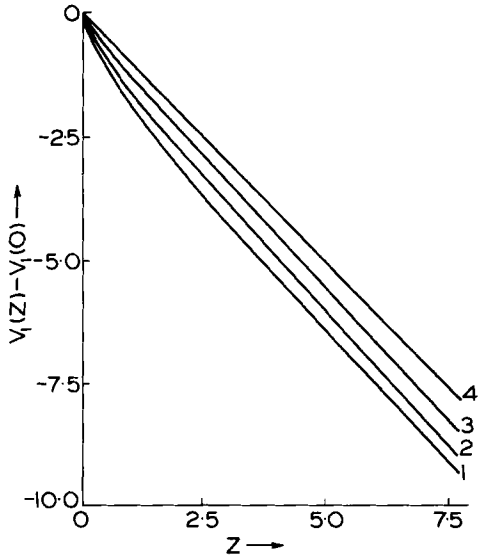

FIG. 4. The voltage drop $V_1(z) - V_1(0)$ is plotted as a function of z. Curve 1 is for the FCVD method. Curves 2, 3, and 4 are for the PVD method with $C = 2$, 0.5, and 0, respectively.

junction. This situation is identical to a forward-biased diode in which the excess carriers are injected only at the junction.

From a practical point of view, the main interest in the OCVD experiments is in the determination of τ_b from the slope of the linear region of the OCVD (PVD or FCVD) curve by using Eq. (82). The value of τ_b thus obtained will be correct provided the slope of $V_1(z)$ versus z curve as given by Eq. (81) or Eq. (89) is unity. The slope is unity only in a certain mathematical limit as shown above. We therefore examine how much the slope of $V_1(z)$ versus z curve differs from unity in case of PVD and FCVD.

Figure 5 shows the variation of slope $dV_1(z)/dz$ with C for different values of z as calculated from Eq. (87). This figure also shows the slope for the FCVD curve. The main features of this figure, as observed by Jain (1981), are given below.

1. Slopes for FCVD as well as PVD are always larger than unity. The resulting values of lifetime will therefore be smaller than τ_b. This error reduces progressively with increasing z, for example, from 180% at $z = 0.25$ to 17% at $z = 2.25$ in case of FCVD. For a reasonable estimate of τ_b therefore, the slope should be measured for $z > 2.25$, provided, of course, the voltage has not decayed to such a low value that the space-charge and junction capacitance efforts become important and the inequality (79) is violated.

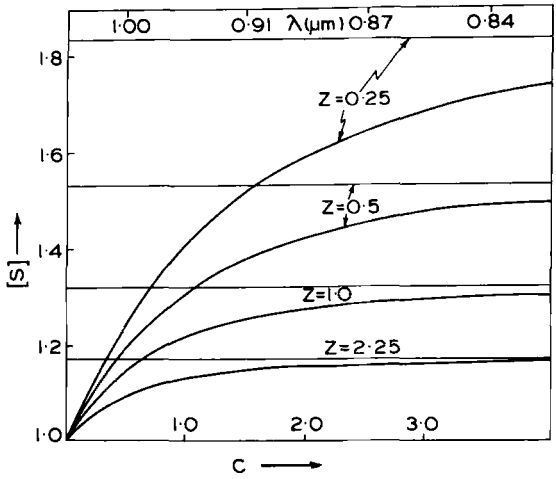

FIG. 5. The values of slope S are plotted as a function of the parameter C for four different values of time z. Assuming a value of 50 μm for L_b, the corresponding values of λ are also shown in the figure.

2. For small values of C, the slope of the PVD curve is relatively closer to unity. For example, at $C = 0.2$, the slope differs from unity by 10% at $z = 0.5$ and 6% at $z = 2.25$. A small value of C corresponds to a low absorption coefficient and therefore a large wavelength of light (see, for example, Agarwala *et al.*, 1980, for a discussion of data on absorption coefficient). For a silicon solar cell, Jain (1981) has recommended that light of wavelength 0.9–1.1 μm will be most useful for determination of τ_b.

In Jain's (1981) analysis as reviewed above, it has been assumed that the steady state had been reached before $t = 0$. In actual experiments light flashes are obtained by using stroboscopes and duration of flashes may not be long enough for the excess carriers to attain their steady-state profile before the decay starts. The analysis given above applies to the case when the duration of the light flash is effectively semiinfinite and light intensity falls to zero instantaneously at $t = 0$. We now consider the other extreme case when the duration of the flash is zero but its intensity is infinite. Such a pulse can be mathematically represented by a δ function. This case has been treated by Dhariwal and Vasu (1981) and Muralidharan *et al.* (1982).

The mathematical treatment of the δ function pulse is quite simple and will not be described here (see Dhariwal and Vasu, 1981; Muralidharan *et al.*, 1982). One main result reported in these two papers is that the linear term in the PVD curve is identical to that obtained in the long-pulse case and therefore does not depend upon the duration of the pulse.

Muralidharan *et al.* (1982) have found that for small values of C, the behavior of the short-pulse (δ function)-induced PVD and the long-pulse-induced PVD is quite similar. As C increases the initial part of PVD curve in both the long- and short-pulse cases becomes curved. The increase in curvature is much larger for the short-pulse-induced PVD than that for the long-pulse case. Lifetime τ_b can be determined from the slope of the linear region in either case. However, in the short-pulse case, the initial curvature of the PVD curve will become quite large at the cost of the linear region. The large C values or light of short wavelengths are therefore less useful for the short-pulse-induced PVD.

In general, for small values of C and for a thick solar cell, it would be quite advantageous to use short-pulse excitation for inducing PVD. The practical utility of this result lies in the fact that GaAs laser diodes can be used for PVD experiments in silicon solar cells. The pulse width in these lasers is about 0.1 μsec. This pulse can therefore be regarded as a δ function pulse since its width is much smaller than τ_b in silicon, which is of the order of a few microseconds.

Before closing this section we shall mention a rather important difference between FCVD and PVD. We consider the time derivative of the voltage decay curve at z close to zero. Using the McLaurin's expansion of $\operatorname{erfc}\sqrt{z}$ (Abramowitz and Stegun, 1965), we obtain the following results for FCVD by using Eq. (80):

$$\Delta V_1(z) = -\frac{2}{\sqrt{\pi}}\sqrt{z} + \cdots \tag{91}$$

and

$$\frac{dV_1(z)}{dz} = -\frac{1}{\sqrt{\pi z}} + \cdots \tag{92}$$

Similarly, by using Eq. (85) we obtain the following for PVD:

$$\Delta V_1(z) = -(C+1)z + \cdots \tag{93}$$

We observe from Eqs. (91) and (93) that near $z=0$, FCVD curve has a $\sqrt{z}$ dependence whereas PVD has a linear dependence on z. In fact the $\sqrt{z}$ terms in expansions for $S(z)$ and $S(C^2z)$ on the right-hand side of Eq. (87) cancel out exactly. The first derivative of the FCVD curve has a singularity at $z = 0$, which is absent in the PVD curve. The FCVD curve therefore, unlike the PVD, shows a kink at $z = 0$. This kink exaggerates the ohmic drop in the FCVD curve at $z = 0$, which was mentioned at the beginning of Section III.A.

Physically this difference between FCVD and PVD arises because of the following. In an FCVD experiment a finite forward current flows through the junction until the decay starts at $t = 0$. The gradient of the excess carrier

profile is determined from this magnitude of the current which is nonzero. After $t = 0$ when the decay starts, the diode is open circuited. Hence the gradient of the excess carrier profile at the junction is zero. Thus the gradient of the excess carrier profile at the junction has a discontinuity across $t = 0$ in a FCVD experiment.

In contrast, the solar cell in a PVD experiment is in open-circuit configuration before as well as after $t = 0$. The gradient of the excess carrier profile at the junction therefore remains continuous across $t = 0$.

C. *FCVD in Thin Diodes*

FCVD in thin diodes has been discussed in several papers (Muralidharan *et al.*, 1982; Sharma and Tewary, 1982; Joshi and Singhal, 1982; for a review and earlier references, see Nosov, 1969). In this section we shall mainly review the work of Muralidharan *et al.* (1982).

The time-dependent diffusion equation in this case is the same as Eq. (75) with $F_b = 0$. The boundary conditions are given by Eq. (13) and (17) and the initial condition is as given by Eq. (33) with the initial steady-state profile as given by Eq. (46). The solution of the diffusion equation in this case can be obtained by expansion in terms of an appropriate set of orthogonal functions (see, for example, Carslaw and Jaeger, 1959). Taking $F_b = 0$ (no drift field), and using the zero-current condition given by Eq. (76), along with the Shockley condition given by Eq. (29) and the inequality (79) we obtain the following result for FCVD:

$$\exp[\Delta V_1(z)] = \frac{q_{bj}(z)}{q_{bj}(0)} = \sum_r B_r \exp(-\varepsilon_r^2 z) \tag{94}$$

where

$$\varepsilon_r^2 = 1 + \mu_r^2 / W_b^2 \tag{95}$$

and μ_r are the real roots of the following equation:

$$\mu_r \tan \mu_r = S_b^* W_b \tag{96}$$

The coefficients B_r have to be determined from the steady-state profile. We shall give below the expressions for FCVD in the two limiting cases, i.e., $S_b^* = 0$ and ∞.

1. *Ideal BSF Diode* ($S_b^* = 0$)

a. *For Small W_b and Large z.*

$$\exp[\Delta V_1(z)] = e^{-z} \frac{2 \tanh W_b}{W_b} \left[1 + \sum_{r=0}^{\infty} \frac{\exp(-\mu_r^2 z)}{1 + \mu_r^2} \right] \tag{97}$$

where

$$\mu_r = r\pi/W_b$$

The series in Eq. (94) is rapidly convergent for small W_b and large times. An alternative series which is more rapidly convergent for large W_b and short times has also been obtained by Muralidharan *et al.* (1982) and is given below.

b. For Large W_b and Small z.

$$\exp[\Delta V_1(z)] = 1 - \tanh W_b\left[\operatorname{erf}\sqrt{z} - 2\sum_{r=0}^{\infty}\psi_1\{2(r+1)W_b, z\}\right] \quad (98)$$

where the function ψ_1 is defined as

$$\psi_1(x,z) = \frac{1}{2}\left[e^{-x}\operatorname{erfc}\left(\frac{x}{2\sqrt{z}} - \sqrt{z}\right) - e^{x}\operatorname{erfc}\left(\frac{x}{2\sqrt{z}} + \sqrt{z}\right)\right] \quad (99)$$

2. Conventional Diode ($S_b^* = \infty$)

a. For Small W_b and Large z.

$$\exp[\Delta V_1(z)] = \frac{2\coth W_b}{W_b}\sum_{r=0}^{\infty}\frac{\exp[-(1+\mu_r^2)z]}{1+\mu_r^2} \quad (100)$$

where

$$\mu_r = \frac{(2r+1)\pi}{2W_b} \quad (101)$$

b. For Large W_b and Small z.

$$\exp[\Delta V_1(z)] = 1 - \coth W_b\left[\operatorname{erf}\sqrt{z} - 2\sum_{r=0}^{\infty}\psi_1\{2(r+1)W_b, z\}\right] \quad (102)$$

where ψ_1 has been defined by Eq. (99).

Figure 6 shows $\Delta V_1(z)$ versus z curves for different values of W_b and for an ideal and conventional diode. For the purpose of comparison, this figure also gives the FCVD curve for a thick diode as calculated from Eq. (80). The main features of Fig. 6 are given below.

1. In general the decay curves have linear region. For smaller W_b, the linear region in the decay curve sets in earlier. This behavior could be mathematically expected from Eqs. (97) and (100). These equations show that after a sufficiently long time (large value of z), the first term in the series on the right-hand side of Eqs. (97) or (100) will dominate. Then $\Delta V_1(z)$ will be linear in z provided of course the inequality (79) is not violated. For low values of W_b, the first term will start dominating for smaller value of z.

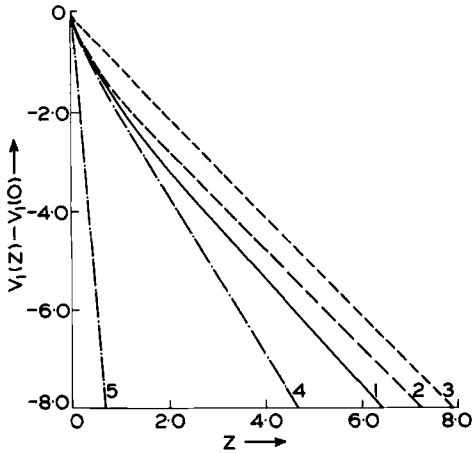

FIG. 6. Plots of $V_1(z) - V_1(0)$ versus z for the FCVD method. Curve 1, $W = \infty$, $S = 0$; curve 2, $W = 2.0$, $S = 0$; curve 3, $W = 0.5$, $S = 0$; curve 4, $W = 2.0$, $S = \infty$; curve 5, $W = 0.5$, $S = \infty$.

2. The slope of the linear region is unity for $S_b^* = 0$, whereas it is larger than unity for $S_b^* = \infty$.

The usual practice is to determine τ_b from the slope of the linear region in the FCVD curve by using Eq. (82). For thin diodes, as we have seen above, this relation is not always valid. However, the lifetime determined from the slope by using Eq. (82) can be identified as an effective lifetime τ_{eff}. This can be related to the actual lifetime τ_b by using the slope of the $\Delta V_1(z)$ versus z curve corresponding to the leading terms in the series in Eqs. (97) and (100) as follows:

(*i*) *Ideal BSF Diode* ($S_b^* = 0$)

$$\tau_{eff} = \tau_b \tag{103}$$

(*ii*) *Conventional Diode* ($S_b^* = \infty$)

$$\frac{1}{\tau_{eff}} = \frac{1}{\tau_b}\left(1 + \frac{\pi^2}{4W_b^2}\right) \tag{104}$$

Equation (104) has also been derived by Nosov (1969). This equation shows that the discrepancy between τ_{eff} and τ_b progressively increases as W_b decreases, although the extent of linearity in the FCVD increases as W_b decreases.

In general for intermediate values of S_b^* between 0 and infinity, the nature of the FCVD curves would depend upon both S_b^* and τ_b. It is possible in

principle to obtain S_b^* and τ_b by fitting experimental FCVD curves with theory. It is not quite apparent that such a fitting procedure would yield unique and therefore reliable values of S_b^* as well as τ_b even if the thickness of the diode is accurately known. However, an approximate formula, as given below, can be derived for the effective lifetime in the limiting case when $S_b W_b$ is small but S_b^*/W_b is large:

$$\tau_{eff} = W_b \tau_b / S_b^* \tag{105}$$

The usefulness of the above formula is limited to the case of a very thin diode containing a strong BSF.

D. PVD in Thin Solar Cells

In this section we shall discuss the effects of cell thickness, surface recombination velocity at the back surface (BSF), wavelength of light used for inducing PVD, and drift field on the PVD rates in a thin solar cell. First we shall consider a long-pulse-induced PVD in which the solar cell reaches a steady state before the illumination is switched off at $t = 0$. The case of a short-pulse-induced PVD will be considered later.

The time-dependent diffusion equation for $z > 0$ in the present case is same as Eq. (75) since the illumination is assumed to have been switched off at $z = 0$. The boundary and the initial conditions are as prescribed by Eqs. (13), (17), and (33) and the steady-state ECP as given by Eq. (65) or (69) with appropriate modifications for a constant drift field. The effect of drift field is included by using the transformation given by Eq. (48). For a nonzero drift field, the boundary condition at the back surface as given by Eq. (13) is modified as follows:

$$\left[\frac{\partial q_b(X, z)}{\partial X}\right]_{W_b} + (2F_b + S_b^*) q_b(W_b, z) = 0 \tag{106}$$

The solution of the diffusion equation is obtained by using the transformation given by Eq. (48) and then using the method of expansion in orthogonal functions as in the preceeding section. The required expression for FCVD can then be obtained by using the zero-current condition, i.e., Eq. (21) (ignoring the emitter contribution), the Shockley voltage condition, i.e., Eq. (29), and, for practical convenience, the inequality (79). Following these steps, the result obtained by Sharma and Tewary (1982) is

$$\exp[\Delta V_1(z)] = \sum_r A_r (\mu_r / W_b) \exp(-\varepsilon_r^2 z) \tag{107}$$

where

$$\varepsilon_r^2 = 1 + F_b^2 - (\mu_r / W_b)^2 \tag{108}$$

and μ_r are the solutions of the following equation:

$$\frac{S_b^* \mu_r}{W_b} + \left[\left(\frac{\mu_r}{W_b}\right)^2 - F_b(F_b + S_b^*)\right] \tanh \mu_r = 0 \tag{109}$$

The coefficients A_r are obtained in terms of the excess carrier profile in the steady state.

As in the preceeding sections, the linear region in the $\Delta V_1(z)$ versus z curve will be obtained when the first term in the series on the right-hand side of Eq. (107) dominates. The slope of the linear region, corresponding to the leading root μ_0, is given by

$$\varepsilon_0^2 = 1 + F_b^2 - (\mu_0/W_b)^2 \tag{110}$$

which gives the following expression for the effective lifetime

$$\frac{1}{\tau_{eff}} = \frac{1}{\tau_b}\left[1 + F_b^2 - \left(\frac{\mu_0}{W_b}\right)^2\right] \tag{111}$$

We shall now discuss the effect of various parameters on PVD.

1. Effect of S_b^*, C, and W_b for $F_b = 0$

If $S_b^* = 0$ then all the roots of Equation (109) are imaginary. They are given by

$$\mu_r = ir\pi \qquad (r = 0, 1, 2, \ldots)$$

and

$$\tau_{eff} = \tau_b \tag{112}$$

On the other hand, if $S_b^* = \infty$ then

$$\mu_r = (2r + 1)\pi i/2 \qquad (r = 0, 1, 2, \ldots)$$

and

$$\frac{1}{\tau_{eff}} = \frac{1}{\tau_b}\left[1 + \frac{\pi^2}{4W_b^2}\right] \tag{113}$$

The PVD curves as calculated from Eq. (107) by Muralidharan *et al.* (1982) for different values of C, W_b, $S_b^* = 0$, and ∞ have been shown in Fig. 7. The FCVD curves have also been given in this figure for the sake of comparison. The curves for $W_b = \infty$ have also been included to estimate the validity of the infinite base approximation in the calculation of decay rates.

It may be observed that for $S_b^* = 0$, the PVD curve becomes identical to the FCVD curve for large C and W_b. As C and/or W_b decreases, the initial slope of PVD curves for $S_b^* = 0$ decreases. In this case, the difference between PVD and

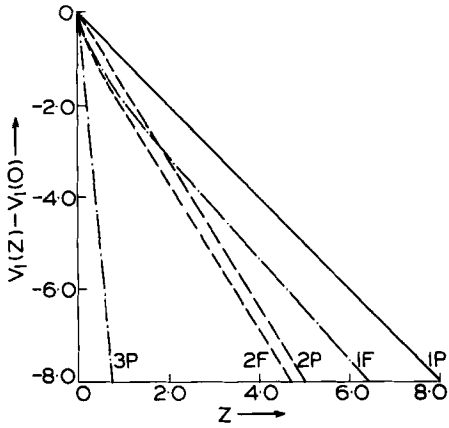

FIG. 7. Plots of $V_1(z) - V_1(0)$ versus z: Line 1P, PVD plot for $C = 0$, $W = \infty$; curve 1F, FCVD plot for $W = \infty$; line 2P, PVD plot for $C = 0$, $W = 2.0$, $S = \infty$; curve 2F, FCVD plot for $W = 2.0$, $S = \infty$; line 3P, FCVD and PVD plot for all values of C, $W = 0.5$, $S = \infty$.

FCVD is maximum when W_b is large and C is small, corresponding to the wavelength of light being large. In such conditions, PVD is more convenient for a measurement of τ_b as compared to FCVD because of the more pronounced linear region in PVD curves.

For a conventional solar cell with $S_b^* = \infty$, Fig. 7 shows that the difference between FCVD and PVD is smaller for $W_b = 2$ as compared to that for $W_b = \infty$. For larger values of C, the difference between PVD and FCVD would decrease even further. For $W_b = 0.5$, the difference between FCVD and PVD is negligible.

2. *Effect of Drift Field on PVD*

The effect of drift field on PVD has been calculated by Sharma and Tewary (1982). They find that in general PVD is sensitive to the magnitude as well as the sign of the drift field F_b. A positive F_b refers to the retarding field whereas a negative F_b refers to the accelerating field. A retarding field drives the carriers toward the junction and thus retards the decay of the voltage. On the other hand, an accelerating field drives the carriers away from the junction and thus accelerates the voltage decay.

Mathematically this behavior can be seen from Eq. (109). We will consider a conventional solar cell with $S_b^* = \infty$. For this case, Eq. (108) reduces to

$$\mu_r = F_b W_b \tanh \mu_r \tag{114}$$

For negative F_b, Eq. (114) will have no real root except $\mu_0 = 0$. This will give the smallest decay constant ε_0 in Eq. (108) since the imaginary values

of μ_r will make a positive contribution to ε_r^2. Hence $r = 0$ will give the leading decay mode. The value of ε_0 as obtained from Eq. (108) for $\mu_0 = 0$ is

$$\varepsilon_0^2 = 1 + F_b^2 \tag{115}$$

For a retarding field ($F_b > 0$), Eq. (114) can have real roots. The largest real root will give the leading mode of decay. We consider the limit of a very strong retarding field such that

$$F_b W_b \to \infty$$

In this limit the real root of Eq. (114) corresponding to the leading mode μ_0 is given by

$$\mu_0 \approx F_b \mu_b \to \infty \tag{116}$$

The corresponding value of ε_0^2 as obtained from Eq. (108) is

$$\varepsilon_0^2 = 1 \tag{117}$$

which gives, from Eq. (107),

$$\Delta V_1(z) = -z + \ln A_0 F_b \tag{118}$$

and from Eq. (111)

$$\tau_{eff} = \tau_b \tag{119}$$

Thus, we get an interesting result as derived by Sharma and Tewary (1982) that, in the limit of a very strong retarding field, the slope of the linear region of the PVD curve becomes independent of the field as well as the thickness of the base. Physically this result can be understood as follows. A retarding field opposes the diffusive loss of excess carriers at the junction. It can not create or destroy the carriers. After the field is large enough to totally counteract the diffusion process, a further increase in the field would have no effect on the excess carrier concentration at the junction. In this limit the excess carrier concentration at the junction will decay by recombination only, which gives unity slope in the $\Delta V_1(z)$ versus z curve and $\tau_{eff} = \tau_b$.

Figures 8 and 9 show PVD curves for different values of F_b and W_b as calculated by Sharma and Tewary (1982). These curves show that the effect of accelerating field is relatively larger for large values of W_b. Physically, it happens because, for large values of W_b, the gradient of the excess carrier profile at the junction is small. Hence the diffusive loss is reduced and the effect of the accelerating drift field becomes relatively more pronounced. For small W_b the excess carrier profile for $S_b^* = \infty$ becomes more steep so that the diffusion process becomes stronger and the relative effect of the field is less significant. For $S_b^* = 0$, a smaller W_b will not increase the "steepness" of the excess carrier profile and this effect will not be there.

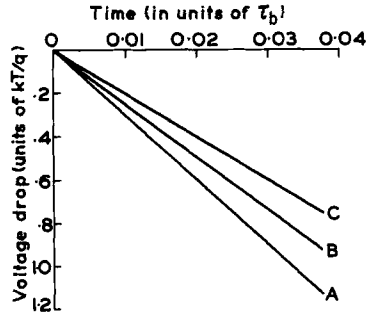

FIG. 8. Effect of drift field on PVD ($W = 0.1$, $C = 1$). For curves A, B, and C, $2F = -5$, 0, and 5, respectively.

The main conclusion of this analysis is that for small W_b (≈ 0.5), PVD and FCVD are almost identical both for solar cells with $S_b^* = 0$ (ideal BSF) and $S_b^* = \infty$ (conventional solar cell). The slope of the linear region would depend strongly on S_b^*. For $S_b^* = 0$ the slope is unity for FCVD as well as PVD, irrespective of the values of C and W_b as long as W_b is not too large. For $S_b^* = \infty$ the slope is $1 + \pi^2/4W_b^2$ as given by Eq. (113), which increases as W_b decreases.

In general, the infinite base approximation is better for low values of time. This is physically obvious because the carriers, after diffusing away from the junction, will take a finite time to "feel" the presence of the other end. The validity of the infinite base approximation for $S_b^* = \infty$ also depends upon the relative magnitudes of C and W_b. For large C the infinite base approximation would become reasonable for smaller W_b. This can be physically understood by recalling that a larger C implies a smaller absorption length. Sharma and

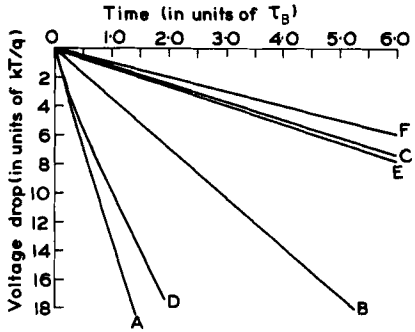

FIG. 9. Effect of drift field on PVD ($C = 1$). For curves A, B, and C, $2F = -5$, 0, and 5, respectively, and $W = 1$. For curves D, E, and F, $2F = -5$, 0, and 5, respectively, and $W = 3$.

Tewary (1982) find that, in general, for reasonable values ($C > 0.1$) the infinite base approximation becomes reasonable for $W_b > 3$.

We shall now briefly describe PVD induced by a short light pulse in which the duration of the illumination is not long for the solar cell to reach a steady state. Before proceeding further we note from Eq. (94) and Eq. (107) that the decay rates (coefficients of z in the exponents) are determined from the geometry and the characteristics of the device. They are same for FCVD as well as PVD and would not depend upon the nature or duration of the illumination.

The coefficients A_r, i.e., the expansion coefficients in the series in Eq. (94) and Eq. (107) are determined from the excess carrier profile in the steady state, which of course depends upon the nature as well as the duration of illumination. These coefficients essentially determine the initial curvature of the decay curve and the onset of the linear region. The slope of the linear region from which the lifetime is determined does not depend upon the characteristics of the steady state and therefore neither on the nature nor the duration of the illumination.

We infer therefore that the slope of the linear region in the PVD curve will remain the same irrespective of whether a short or a long pulse has been used for inducing the PVD. A detailed calculation of PVD induced in a thin solar cell by a δ function pulse has been carried out by Muralidharan *et al.* (1982). Both ideal BSF type ($S_b^* = 0$) and the conventional solar cells with ohmic contact at the back ($S_b^* = \infty$) have been considered. These results are shown in Fig. 10.

Fig. 10 also gives PVD curves for $W_b = \infty$. It may be observed that for $W_b = \infty$ the short-pulse-induced PVD curve lies above the FCVD curve for $C < 1$ and below it for $C > 1$. At the other extreme, the PVD curve for a short pulse does not depend upon the value of C for $W_b = 0.5$ and $S_b^* = \infty$ and is identical to the FCVD curve.

E. Limitations of the OCVD Method for Lifetime Determination and Small Signal OCVD

In the preceding section we have obtained various expressions for voltage decay in diodes and solar cells. These expressions can be used for determination of the excess carrier lifetime in the base of a device. There are, however, some limitations which are summarized below.

1. Variation of Lifetime

During the time of a typical OCVD experiment the excess carrier concentration near the junction varies by a large amount. The junction voltage

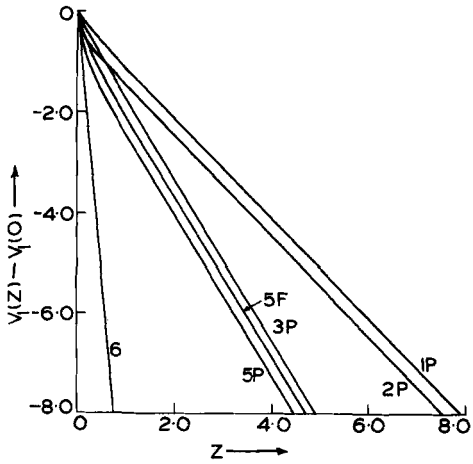

FIG. 10. Plots of $V_i(z) - V_i(0)$ as a function of z. Curve 1P, PVD after short-pulse excitation plot for $W = 0.5$, $S = 0$, $C = 0.5$; curve 2P, PVD after short-pulse excitation plot for $W = 0.5$, $S = 0$, $C = 2.0$; curve 3P, PVD after short-pulse excitation plot for $W = 2.0$, $S = \infty$, $C = 0.5$; curve 5F, FCVD plot for $W = 2.0$, $S = \infty$; curve 5P, PVD after short-pulse excitation plot for $W = 2.0$, $S = \infty$, $C = 2.0$; curve 6, FCVD and PVD after short-pulse excitation plot for all values of C, $W = 0.5$, $S = \infty$.

varies say from 0.6 to about 0.3 V. The excess carrier concentration which is proportional to $\exp(qV/kT)$ will therefore vary by 3–4 orders of magnitude at room temperature. The excess carrier concentration also has a strong spatial dependence and will vary from a high value near the junction to zero at the back ohmic contact. Except when the excess carrier concentration remains sufficiently high or sufficiently low during the course of an experiment, the excess carrier lifetime will also vary (see Section II.B). The theory developed in the preceeding section does not account for this variation. An attempt to account for the variation of excess carrier lifetime in space and time will necessarily require solving a nonlinear differential equation.

2. *Diode Factor and Its Variation*

In the Shockley boundary condition given by Eqs. (28) and (29) the exponent is qV_j/kT. In general, in a real case, the exponent can be written as qV_j/AkT where A is called the diode factor. A is equal to unity in the ideal case of a Shockley diode but otherwise varies between 1 and 2 or even more. There is a considerable uncertainty in the actual value of A. If A is taken to be a constant then the derivations given in Section III.B would yield A/τ_b as the slope of the linear region in the OCVD curve. Since the lifetime is determined from the slope of the linear region, any uncertainty in A directly affects the

determination of the lifetime. The situation is worse if A is taken to be a function of time, which again makes the diffusion equation nonlinear.

3. *High Injection Effects*

The effect of high injection is to modify the excess carrier lifetime as well as the diode factor. In addition, it causes a saturation of the junction voltage (Dhariwal *et al.*, 1976; Fletcher, 1957) which is described by the nonlinear boundary conditions as given in Section II.C. Consequently, the expressions given in this article, i.e., Sections III.A–D for OCVD are not valid. Moreover, as we shall see in Section VI the effect of p–n coupling becomes quite important at high injections but this has been neglected in the present formulae given in the this section. In general, in a typical silicon diode or solar cell, the high injection effects may become important when the junction potential exceeds 0.6 V.

4. *Low Injection Effects*

At low junction voltages, the space-charge effects and the junction capacitance leakage effects become significant. These effects have not been included in the present theory. Moreover, the linear region in the OCVD curve would exist only if the inequality (79) is satisfied. This inequality is of course violated at much lower voltages than that when the space-charge effects set in. In a typical silicon diode or a solar cell, the space-charge effects become significant when the junction voltage drops to lower than 0.4 V.

The factors given above cause severe limitations on the determination of excess carrier lifetime by the OCVD method. The starting voltage should not be too high to avoid high injection effects. The linear region in the decay curve from which the lifetime is determined occurs only after some time but during this time the voltage should not drop to too low a value to avoid space-charge effects. The voltage-decay range should not be too large to avoid the variation of the excess carrier lifetime. Yet it should be large enough for the linear region to be identified. Moreover, the diode factor in this region should be accurately known.

Some of the aforementioned difficulties can be avoided by using what is called the small-signal OCVD method in solar cells. This very useful and elegant method was suggested by Moore (1980) and is briefly described below.

We consider a base-dominated solar cell illuminated by stationary light so that it is in steady state with open-circuit voltage V_{sj}. In this state a pulse of light is applied to the solar cell. It may be a long pulse so that the junction voltage reaches a new steady-state value $V_{sj} + V_{0j}$ which eventually decays to V_{sj}. It may also be a short δ function type pulse so that the junction voltage reaches its peak value $V_{sj} + V_{0j}$ and then decays to V_{sj}.

Let q_{sj} denote the excess carrier concentration at the junction in the initial steady state corresponding to the voltage V_{sj}. The additional excess carrier concentration at the junction corresponding to the additional voltage V_{0j} is denoted by q_{0j}. We now make the small-signal approximation so that

$$V_{0j} \ll \frac{kT}{q} \tag{120}$$

With this approximation, using the mathematical methods given earlier in this chapter, the following formulae for the voltage decay can be easily derived (see Moore, 1980):

$$\Delta V_1(z) = \frac{A q_{0j}}{q_{sj}} \chi(z) \tag{121}$$

where A is the diode factor and $\chi(z)$ is a function which represented $q_j(z)$ in the earlier sections of this article. For example, for a thick-base ($W_B = \infty$) solar cell, $\chi(z)$ is the function given by the right-hand side of Eq. (85). Similarly, for a thin solar cell, it is given by the right-hand side of Eq. (107) with ε_r and $B_r = A_r \mu_r / W_b$ as given in Section III.D for different cases. Except in the earliest stages of the decay, the function $\chi(z)$ can be expressed in the following form:

$$\chi(z) = B_0 \exp(-\varepsilon_0^2 z) \tag{122}$$

As discussed in the earlier sections of this article, ε_0 is known quite accurately. In a thick solar cell as well as in a thin solar cell with an effective BSF ($S_b^* = 0$) and no drift field, $\varepsilon_0 = 1$. For other cases the values of ε_0 have been given in Section III.D. Any uncertainties in the starting excess carrier's profile and the duration of the pulse would affect only B_0 and not ε_0. The quantity ε_0 is also independent of the diode factor.

Combining Eqs. (121) and (122) we see

$$\ln \Delta V_1(z) = \text{const.} - \varepsilon_0^2 z \tag{123}$$

We see from Eq. (123) that if the log of the voltage drop is plotted against time, we expect a straight line with slope ε_0^2/τ_b ($z = \tau/\tau_b$). Since ε_0^2 is accurately known, τ_b can be determined from the slope of this straight line. The slope is obviously independent of the diode factor, duration of the pulse, as well as any uncertainties in the starting steady-state excess carrier profile.

The method also has the advantage that the decay range is small, i.e., $V_{sj} + V_{0j}$ to V_{sj}. The lifetime can be easily assumed to be constant within this range. The measurements are effectively made at the chosen value of V_{sj}. Thus by taking different values of V_{sj} corresponding to different intensities of the stationary light, we can measure the dependence of the excess carrier lifetime on the intensity of the illumination, i.e., the level of injection. It

may be remarked that V_{sj} should be chosen such that it is neither too high nor too low so that high injection effects as well as space-charge effects are not significant.

F. Interpretation of Experimental Results on PVD

FCVD in diodes has been a popular technique for measurement of excess carrier lifetime as well as series resistance of the diode for several years (see, for example, Nosov, 1969). In contrast PVD is a new technique and very few experimental papers on PVD are available in the literature. Perhaps the first experimental results on PVD in solar cells were published by Mahan *et al.* (1979). Subsequently, more experimental work has been reported by Ray *et al.* (1982), Madan and Tewary (1983), and Moore (1980) on small-signal PVD.

The usual electrical circuit for PVD measurements is quite similar to that for FCVD. For illuminating the solar cell, Mahan *et al.* (1979) used an electronic stroboscope. They used a composite light source but the spectral composition of the light used was not reported. Hence it has not been possible to make a quantitative comparison between the theory and their experimental results.

The main qualitative features of the experimental results of Mahan *et al.* are given below.

1. The voltage decay curves are more linear in case of PVD as compared to those for FCVD.
2. The photo induced voltage persists for a longer duration.
3. The values of lifetimes as determined by the PVD method are considerably larger than those obtained by the FCVD method.
4. The values of lifetime obtained by the PVD method seem to be more accurate than those obtained by the FCVD method.

The above qualitative features are consistent with those predicted by Jain's (1981) theory. This can be seen from Fig. 4. As mentioned in Section III.B, the infinite value of C in PVD corresponds to FCVD. We see from Fig. 4 and as already mentioned in Section III.B as C decreases, the PVD curves become more linear and the slope of the linear region comes closer to unity. Thus we see that compared to infinite value of C, i.e., the FCVD method, a finite value of C, i.e., the PVD method will give more pronounced linear region (observation 2), smaller slope (observation 3), and more accurate value of the lifetime (observation 4). Figure 4 also shows that PVD curves are above the FCVD curve, which is consistent with observation 2.

A more quantitative verification of the theory is possible by using the experimental results of Madan and Tewary (1983). They have obtained PVD

curves for monochromatic light of wavelengths of 690, 590, 560, 500, 410 nm, and also for composite light. Their results are shown in Fig. 11. The monochromatic beams of light were obtained by using interference filters. The initial open-circuit voltage for each wavelength is a measure of intensity of steady-state illumination.

By a detailed analysis, Madan and Tewary (1983) infer that their curves can be compared with the theories of Jain (1981) or Dhariwal and Vasu (1981) until about 0.4 V. Below this voltage the low injection effects, e.g., space-charge effects, become significant. Since curve 6, i.e., the one corresponding to wavelength 410 nm starts at just about 0.4 V, it cannot be analyzed by using the existing theories.

The remaining curves (1–5) in Fig. 11 all become linear and parallel to each other after about 20 μsec and remain so until the voltage drops to about 0.4 V. The slopes of the linear region in all these curves do not differ by more than 20%. These features are consistent with the theories of Jain (1981) as well as those of Dhariwal and Vasu (1981). The lifetime determined from this slope comes out to be about 23 μsec, which seems to be a reasonable value.

However, a more detailed analysis shows that in the initial region of high curvature, the experimental PVD curves as obtained by Madan and Tewary (1983) differ considerably with those predicted theoretically by Jain (1981) and Dhariwal and Vasu (1981). Madan and Tewary (1983) attribute this discrepancy to the following two factors:

1. Jain's (1981) theory assumes a long pulse so that a steady state is assumed to have reached before the decay starts. On the other hand, Dhariwal

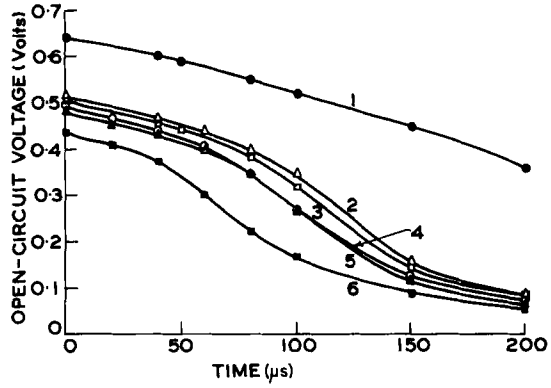

FIG. 11. Spectral dependence of the PVD in a silicon solar cell for composite light (curve 1) and for wavelengths of 690 nm (curve 2), 590 nm (curve 3), 560 nm (curve 4), 500 nm (curve 5), and 410 nm (curve 6).

and Vasu (1981) assume a δ function pulse. Neither of these assumptions are valid for the pulse used in the experiment.

2. The thick-base and zero-drift-field approximations may not be valid in the solar cell used in the experiment.

Sharma and Tewary (1982) have also analyzed the experimental results of Madan and Tewary (1983) on the basis of their theory of PVD in a thin solar cell. This theory has been described in Section III.D. They have fitted the experimental results with Eq. (107) by using a least square fitting procedure and thus obtained the best values of τ_b, L_b, d_b, and F_b. Two different sets were obtained. In one set the drift field F_b was forced to be zero whereas in the other set, F_b was assumed to be finite and constant. These values are given below:

Set 1: $\tau_b = 47\ \mu\text{sec}$, $L_b = 458\ \mu\text{m}$, $d_b/L_b = 1.57$, $F_b = 0$

Set 2: $\tau_b = 23\ \mu\text{sec}$, $L_b = 128\ \mu\text{m}$, $d_b/L_b = 1.55$, $F_b = 3.85$

It can be easily verified that both these sets are consistent with the effective lifetime as defined by Eq. (109). The value of τ_{eff} in the present case, as obtained from the slope of the region and as quoted earlier, is 23 μsec.

The fit between the theoretical and experimental results using the parameters of Set 1 is shown in Fig. 12. A similar fit is obtained by using Set 2. Although the theoretical results fit well with the experimental results they obviously do not yield a unique set of values for the parameters. It is therefore

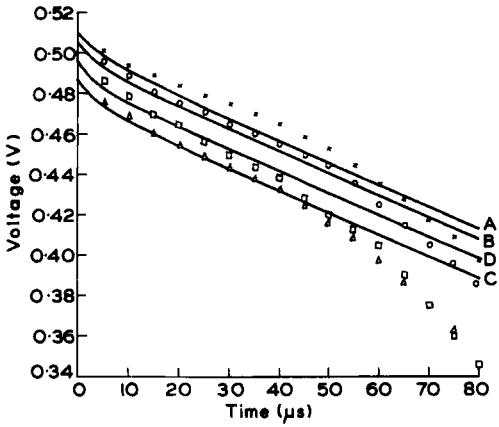

FIG. 12. Fitting of theory with the experimental data on PVD assuming zero-drift field. Curves A, B, C, and D correspond to light wavelengths (in nm) of 690, 590, 560, and 500, respectively. The corresponding experimental points are shown by ×, ○, △, and □, respectively.

essential to have independently measured values of some of the parameters to obtain a reliable value of τ_b.

The experimental results obtained by Moore (1980) on small-signal PVD are shown in Fig. 13. Two small-signal PVD curves, one with and the other without stationary light bias, are shown in the figure. It may be seen that the PVD curve without the stationary light bias is not exponential, presumably due to space-charge effects. The small-signal PVD curve with a stationary light bias is indeed exponential as predicted theoretically (see Section III.E). The slope of the linear curve plotted on a log graph gives $\tau_b = \sim 7$ μsec by using Eq. (123) taking $\varepsilon_0 = 1$.

Using this technique, Moore (1980) has experimentally obtained the dependence of τ_b on the level of injection. Moore (1980) finds that in a particular solar cell, τ_b increases from 7.5 μsec at a light intensity of 3.8×10^{-3} Sun (equivalent) to 26 μsec at light intensity of 0.4 Sun (equivalent). It then decreases to 8.2 μsec as the light intensity further increases to 40 Sun (equivalent). Moore (1980) has also given an explanation of the observed dependence of τ_b on the injection level in terms of the Shockley–Reed–Hall two-level recombination mechanism.

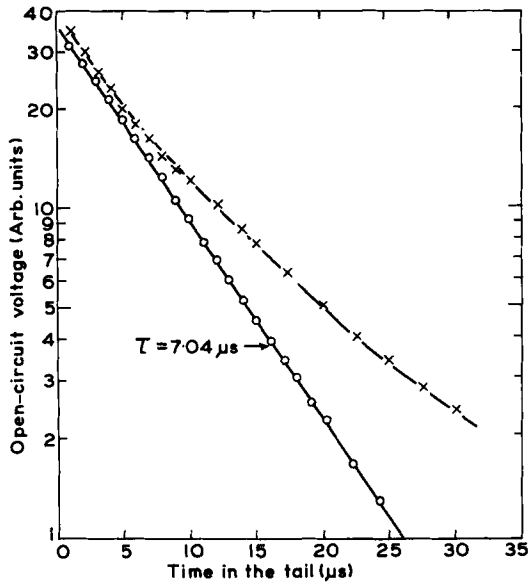

FIG. 13. Open-circuit voltage in the tail of the decay. The upper curve is with no light bias, the lower curve is with a small light bias equivalent to less than 0.1 mA short-circuit current. The normal operating range of these cells is near 1 A. ×, No light bias; ○, with light bias.

IV. Effect of Emitter on OCVD

In the previous section we discussed OCVD in base-dominated devices. In such devices the effect of the emitter is negligible. This approximation is valid in a device in which the injection efficiency of the emitter is close to unity, i.e., the saturation current of the emitter is much less than the saturation current in the base.

Most of the early work on characteristics of the devices was done on base-dominated devices in steady state (see, for example, Shockley, 1950, and various papers in Backus, 1976) as well as transient state (Gossick, 1955; Lederhandler and Giacoletto, 1955; Kingston, 1954; also the work reviewed by Nosov, 1969). The effect of stored charges in the emitter was discussed by Lederhandler and Giacoletto (1955) but this work was not pursued further. This was presumably because the injection efficiency of the emitter was indeed close to unity in the germanium diodes that were mostly used in 1950s.

In a typical modern silicon device the emitter is heavily doped. As mentioned in Section I.B, the heavy and nonuniform doping of the emitter causes band-gap shrinkage which increases the saturation current of the emitter. In such devices the effect of the emitter becomes quite important. This was recognized by Lindholm and Sah (1976) for transient characteristics and Fossum *et al.* (1979; also see Sharma *et al.*, 1981) for steady-state characteristics of devices. The experimental results of Mahan *et al.* (1979) also seem to support this. Subsequently, the effect of emitter on OCVD has been the subject of many papers. Some of these will be reviewed in this and the following sections.

The effect of the emitter on OCVD arises from what is called p–n coupling. The nature and effect of p–n coupling is described in Section IV.A. The effect of p–n coupling on OCVD is likely to be significant in a device in which heavy doping in the emitter results into band-gap shrinkage. Even in a device in which there is no band-gap shrinkage in the emitter and in which the saturation current of the emitter is much less than that of the base, the effect of p–n coupling becomes important at very high injections. This will be discussed in Section VI.

A. p–n Coupling

Consider a p–n junction device in which some excess carriers have been injected. The excess carrier concentrations at the junction on both of its sides are related through the voltage boundary conditions given in Section II.C.3. The excess carrier concentrations in the emitter and the base therefore cannot decay independently of each other. The ECC at the junction, i.e., the heights of

ECP at the junction on both of its sides are coupled with each other through the voltage boundary condition.

Further, the total current through the junction consists of two parts, the emitter current and the base current. The diffusion current is proportional to the gradient of ECP at the junction, whereas the drift current depends upon the height of ECP at the junction. Any physical condition on the current will apply to the total current through the junction and not to the emitter and the base currents individually. In the open-circuit case, for example, the total current has to be zero as given by Eq. (21). Therefore we see that the gradients of the ECP at the junction in the emitter and the base are also coupled.

Thus we see that, during decay, the heights as well as slopes of ECP at the junction in the emitter and the base of the device are coupled together and therefore can not decay independently. This coupling is called p–n coupling since one of the two—emitter and base—would be p type and the other n type. We shall now show qualitatively that the effect of p–n coupling is, in general, to accelerate the voltage decay.

In a typical n^+–p device, for example, the excess carrier lifetime in the emitter may be a few nanoseconds whereas in the base it may be a few microseconds. If the excess carrier concentration in the emitter and the base were to decay independently of each other, decay would be much faster in the emitter than in the base. However, because of the p–n coupling they can not decay independently of each other. The base has to supply enough carriers to the emitter to keep the relative ECC on the two sides of the junction at a value demanded by the voltage condition. The net rate of decay is therefore higher than that from the base alone in the absence of p–n coupling.

In the following subsections of this section we shall discuss the effect of p–n coupling on FCVD and PVD at low injections. Some experimental results will also be discussed. The effect of p–n coupling at high injection will be discussed in Section VI.

B. FCVD in Thick Diodes with p–n Coupling

The theory given in this section is due to Tewary and Jain (1983). We consider the model described in Section II.A (see Fig. 1). We assume a thick diode (or a solar cell used as a diode), i.e., the thickness of the emitter as well as the base is infinite in the sense given in Section II.A. The steady state is assumed to persist until $t = 0$ when the forward current is switched off and the decay starts.

The ambipolar diffusion equations for the emitter and the base in the low injection approximation in terms of the dimensionless variables X_e, X_b, and z

reduce to the following (see Section II.B):

I. Emitter ($-\infty \leq X_e \leq 0$; $z > 0$)

$$\frac{\partial^2 q_e}{\partial X_e^2} - q_e = \frac{1}{\xi}\frac{\partial q_e}{\partial z} \tag{124}$$

II. Base ($0 \leq X_b \leq \infty$; $z > 0$)

$$\frac{\partial^2 q_b}{\partial X_b^2} - q_b = \frac{\partial q_b}{\partial z} \tag{125}$$

where we have assumed the drift field to be zero and

$$\xi = \tau_b/\tau_e \tag{126}$$

The boundary and initial conditions, as given in Section II.C are as follows:

1. At the ohmic contacts for all z

$$q_e(-\infty, z) = q_b(\infty, z) = 0 \tag{127}$$

2. At the junction ($X_e = X_b = 0$) for all z

$$q_e(0, z) = q_{ej}(z) \tag{128}$$

and

$$q_b(0, z) = q_{bj}(z) \tag{129}$$

3. At $z = 0$ (initial condition)

$$q_e(X_e, 0) = q_{es}(X_e) \tag{130}$$

and

$$q_b(X_b, 0) = q_{bs}(X_b) \tag{131}$$

In addition we shall use the following voltage and current conditions as given by Eqs. (28), (29), and (21):

$$q_{ej}(z)/q_{e0} = q_{bj}(z)/q_{b0} = \exp[qV_j(z)/kT] - 1 \tag{132}$$

and

$$\frac{L_e}{\tau_e}\left[\frac{\partial q_e(X_e, z)}{\partial X_e}\right] - \frac{L_b}{\tau_b}\left[\frac{\partial q_b(X_b, z)}{\partial X_b}\right]_{X_b = 0} = 0 \tag{133}$$

In order to obtain the expression for voltage decay i.e., $V_j(z)$ as a junction of z, we solve Eqs. (124) and (125) subject to the boundary and the initial conditions as given above. The solution can be easily obtained by using the standard Laplace transform method (see, for example, Carslaw and Jaeger,

1959). Use of Eq. (133) then gives a relation between $q_{ej}(z)$ and $q_{bj}(z)$. Finally, use of Eq. (132) gives the desired expression for $V_j(z)$ as a function of z.

The initial ECP in steady state for the emitter and the base have been given in Eqs. (36) and (37). Using the inequality (79) the following result can be easily obtained:

$$\exp[\Delta V_1(z)] = \frac{1}{b-a}[b\{S(z) - aS(a^2z)\}\exp(-z) - a\{S(\xi z) - bS(b^2\xi z)\}\exp(-\xi z)] \tag{134}$$

where

$$a^2 = \frac{\xi - 1}{j^2\xi - 1} \tag{135}$$

$$b^2 = \frac{j^2(\xi - 1)}{j^2\xi - 1} \tag{136}$$

$$j = J_{b0}/J_{e0} = \frac{D_b L_e q_{b0}}{D_e L_b q_{e0}} \tag{137}$$

and the function $S(z)$ is as defined by Eq. (86).

The right-hand side of Eq. (134) is known as North's expression and was first quoted by Lederhandler and Giacoletto (1955) without giving its derivation or the model and assumptions on which the expression was derived. North's expression as derived above includes the effect of p–n coupling in the sense described at the beginning of this section. We shall now briefly mention the qualitative features of FCVD as predicted by the North's expression.

1. If $j \gg 1$ and $\xi \gg 1$, then Eq. (135) reduces to

$$\Delta V_1(z) = -z + \ln S(z) \tag{138}$$

which is the usual expression for FCVD in base-dominated diodes as given earlier by Eq. (80). In this limit therefore the effect of coupling is negligible and FCVD is not affected by the emitter.

2. We consider the case when

$$j \leq 1 \tag{139}$$

$$\xi \gg 1$$

and

$$j^2\xi \gg 1 \tag{140}$$

Using the above inequalities in Eqs. (134)–(136) we obtain

$$a = 1/j, \qquad b = 1 \tag{141}$$

and

$$\exp[\Delta V_1(z)] = \frac{e^{-z}}{1-a}[S(z) - aS(a^2 z)] \tag{142}$$

It may be remarked that in devices with heavily doped emitters, inequality (139) may be satisfied for two reasons: (i) an increase in q_{e0} [see Eq. (137)] due to band-gap shrinkage and (ii) a decrease in L_e because of decrease in excess carrier lifetime due to Auger recombination, etc., operative at high doping levels.

We note from Eq. (142) that for $a = 0$, i.e., if $j \gg 1$ so that inequality (140) is satisfied, this case reduces to case 1, i.e., Eq. (138). Thus we infer that the terms containing a in Eq. (142) arise due to the p–n coupling.

3. We now consider the large time ($z \gg 1$) behavior of FCVD as given by Eq. (134) assuming that $\xi \gg 1$. In this limit we obtain the following:

$$\Delta V_1(z) = -z + \ln\left[\frac{b(1-a)}{a(b-a)} z^{-3/2} + \cdots\right] \tag{143}$$

For large z the contribution of the second term on the right-hand side of Eq. (143) will be small. Thus we see that, as in the case of base-dominated diodes discussed in Section III, FCVD curve becomes linear in z with slope unity. Obviously the linear region is not affected by p–n coupling. The same result is of course predicted by Eq. (142), which is an approximate form of Eq. (134).

4. Finally we consider the low time ($z \to 0$) behavior of FCVD. By using the low z expansion of $S(z)$ (Abramowitz and Stegun, 1965), we obtain the following result for $z \to 0$:

$$\Delta V_1(z) = -\frac{2(j+1)}{\sqrt{\pi}(j\sqrt{\xi}+1)}\sqrt{\xi z} \tag{144}$$

The effect of p–n coupling will be negligible in the limit of large j, as can be verified by comparing the large j limit of Eq. (144) with the low z limit of Eq. (80). The dependence of the right-hand side of Eq. (144) on ξ for finite values of j therefore arises due to the p–n coupling.

A particularly interesting effect of the p–n coupling can be seen from Eq. (144) by considering the limit $j \ll 1$ but $j\sqrt{\xi} \gg 1$. In this limit, which represents a strong p–n coupling,

$$\Delta V_1(z) = -\frac{2}{\sqrt{\pi}}\frac{\sqrt{z}}{j} \tag{145}$$

Obviously for $j \ll 1$, $\Delta V_1(z)$ will be large. Thus a strong p–n coupling results in a large voltage drop in the FCVD curve near $z = 0$, i.e., in the initial stages of

the decay. This drop is quite sharp because the derivative of $\Delta V_1(z)$ with respect to z is singular at $z = 0$.

The sharp drop predicted by Eq. (145) is called the coupling drop. This drop will exist in a device in which the emitter is heavily doped so that $\xi \gg 1$ and because of band-gap shrinkage $j \ll 1$. The coupling drop will occur within a time which is of the order of τ_e. In most cases τ_e is of the order of nanoseconds whereas τ_b is of the order of a few microseconds. The FCVD curve is mostly observed on a CRO set to a time scale in microseconds. The coupling drop therefore would appear to be almost vertical and will get added up to the ohmic drop caused by the series resistance of the device [see Eq. (74)]. It is therefore important to separate out the coupling drop from the initial vertical drop for the purpose of determining the series resistance of the device.

The qualitative features of FCVD as discussed above will be apparent from Fig. 14 taken from Tewary and Jain (1983). To summarize, the effect of p–n coupling on FCVD is as follows:

1. The initial stages of the decay are sensitive to p–n coupling.
2. The effect of p–n coupling is to make voltage decay faster, i.e., to make a FCVD curve more steep. This effect is more for lower values of j.
3. In certain cases ($j \ll 1$, $j^2\xi \gg 1$) the effect 2 can be quite pronounced. It results in a very rapid drop in the voltage right at the beginning of the decay. This drop, referred to as the coupling drop, will be added to the ohmic drop due to the series resistance of the device.

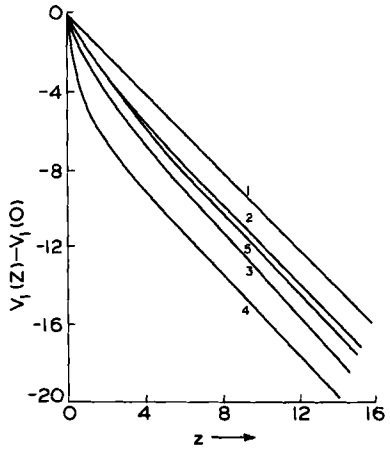

FIG. 14. Reduced voltage $V_1(z) - V_1(0)$ as a function of z. Curve 1 is the ideal linear law, curve 2 is from Eq. (138), curves 3 and 4 are from Eq. (142) for $a = 0.5$ and 10, respectively, and curve 5 is from Eq. (134) for $a = 0.1$ and $b = 0.7$.

4. The large time behavior of FCVD is not sensitive to the p–n coupling. The slope of the linear region in the FCVD curve at large times is determined only by the excess carrier lifetime in the base of the device.

C. *Experimental Results on FCVD Showing the Effect of p–n Coupling*

Madan and Tewary (1985) have carried out a simple experiment which provides at least a qualitative verification of the basic physical ideas underlying the theory described in the preceeding section. Their results clearly show the existence of the coupling drop in the FCVD curve.

As mentioned in Section IV.B, the coupling drop ΔV_c is added to the ohmic drop given by Eq. (74). The total vertical drop ΔV_0 in the FCVD curve at $z = 0$ is therefore given by

$$\Delta V_0 = \Delta V_c + I_F R_s \tag{146}$$

We also define an apparent resistance R^* as follows:

$$R^* = \Delta V_0 / I_F \tag{147}$$

so that, from Eq. (146)

$$R^* = R_s + \Delta V_c / I_F \tag{148}$$

The significance of the apparent resistance R^* should be obvious. It denotes the value of the resistance which would be obtained from the initial vertical drop in the FCVD curve without separating the contribution of the coupling drop. In a device in which ΔV_c is almost 0 (small p–n coupling) R^* will be almost equal to R_s.

From the theory in Section IV.B and also in Section III, it is clear that ΔV_c is independent of I_F. We can also assume that R_s is independent of I_F within the limits that are relevant to our present discussion. Then, Eq. (146) shows that ΔV_0 has a linear dependence on I_F. The slope of this straight line will be as R_s and its intercept with the y axis (ΔV_0 axis) will be equal to ΔV_c. This is obviously in agreement with the experimental results of Madan and Tewary (1985) as shown in Fig. 15. From the slope and the y intercept of the linear region they obtain the following values:

$$R_s = 0.24 \quad \Omega$$

and

$$\Delta V_c = 27 \quad \text{mV}$$

Figure 15 also gives the measured values of the apparent resistance R^*. We see from the figure that the apparent resistance has a hyperbolic dependence

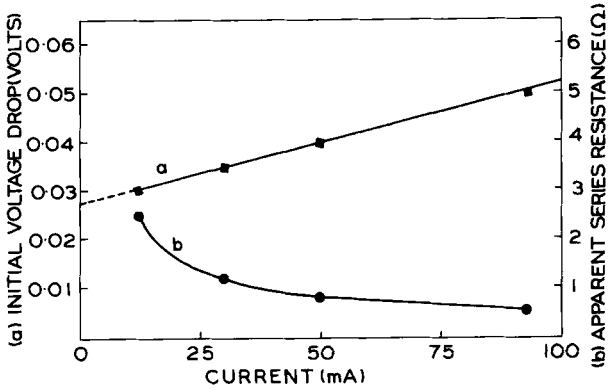

FIG. 15. Initial voltage drop (curve a) and apparent series resistance (curve b) as a function of injection current. Dotted portion of curve a indicates linear extrapolation to zero current.

on I_F as predicted by Eq. (148). For large values of I_F, R^* becomes close to R_s as theoretically expected from Eq. (148). However, if I_F is too large, the high injection effects that have not been included in the theory so far become significant. Also, at very low values of I_F, the low injection effects that have been neglected in the present theory become important. The departure from linearity in the ΔV_0 versus I_F curve at low values of I_F may be due to low injection effects.

For a further verification of the theory, Madan and Tewary (1985) added known additional resistance R_a in series to the diode and measured ΔV_0 for each added resistance. The effect of R_a is obviously to increase the series resistance of the device from R_s to $R_s + R_a$. Using these results, Madan and Tewary (1985) verified that, as expected from Eq. (146), the slope of the ΔV_0 versus I_F line changed from R_s to $R_s + R_a$ but the intercept ΔV_c remained unchanged.

A more direct experimental analysis of the coupling drop can be done by using a high-resolution CRO and adjusting it to the time scale of τ_e (nanoseconds). Such an experiment should be quite interesting and should yield useful information about τ_e.

Madan and Tewary (1985) have also analyzed their FCVD results using Eq. (142), which is a reasonable approximation of the North's expression given by Eq. (135). The experimental and the "best" fit experimental FCVD curves have been shown in Fig. 16. The theoretical curve in this figure was obtained by using a least square fitting procedure which yielded $\tau_b = 11$ μsec and $a = 1.1$.

It may be remarked that the "measured" value of a as reported above may be used to estimate the band-gap shrinkage in the emitter. Let J'_{e0} and

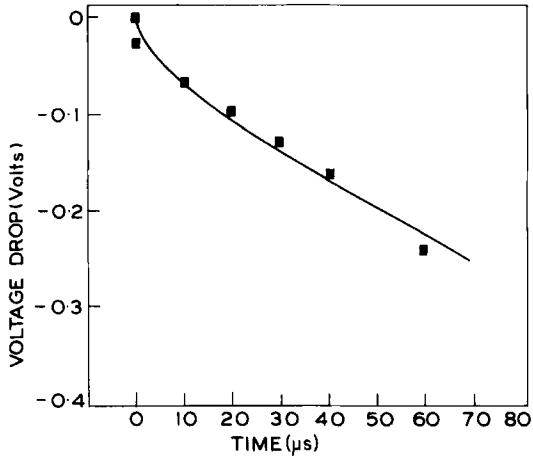

FIG. 16. Calculated open-circuit voltage decay curve in a p–n diode. Points indicate experimental results after subtracting series resistance contribution.

J'_{b0} represent the saturation currents in the emitter and the base of the device, respectively, in the absence of any band-gap shrinkage. J'_{e0} and J'_{b0} can be calculated from the thermal equilibrium values of the carrier concentration (doping levels). If the band-gap shrinkage in the emitter is ΔE_g, then the effective saturation current in the emitter will be given by

$$J_{e0} = J'_{e0} \exp(\Delta E_g / kT) \tag{149}$$

We assume that the base is not heavily doped so that there is no band-gap shrinkage in the base. Then we get from Eqs. (141) and (149).

$$a = a' \exp(\Delta E_g / kT)$$

or

$$\Delta E_g = kT \ln(a/a') \tag{150}$$

where $a = J_{e0}/J_{b0}$ is the value obtained from the FCVD data and $a' = J_{e0}/J'_{b0}$ is the value of a obtained without accounting for band-gap shrinkage. Eq. (150) gives a reasonable estimate of ΔE_g consistent with the FCVD data.

D. Effect of p–n Coupling on OVD in Thick Solar Cells

The effect of p–n coupling on PVD in thick solar cells ($W_b \to \infty$) has been discussed by Sharma *et al.* (1981) and Sharma and Tewary (1983). They have used the same model as shown in Fig. 1 and described in Section II.A. The

time-dependent coupled diffusion equations to be solved in the present case are the same as Eqs. (124) and (125) because the illumination is assumed to have been switched off at $z = 0$.

The boundary conditions at the back of the base ($W_b = \infty$) and at the junction are the same as in the case of FCVD [Eqs. (127)–(129)]. Formally, the initial conditions in the present case are also the same as those given by Eqs. (130) and (131). The ECP in the base for the present case is given by Eq. (57). The ECP in the emitter is somewhat complicated and is not quoted here (see Sharma *et al.*, 1981). The boundary condition at the front of the emitter is as given by Eq. (11) without the second term on the right-hand side. The second term ηN_0 will contribute only in the steady state and not in the transient state after the illumination has been switched off.

The formal solution of Eqs. (124) and (125), subject to the above boundary and initial conditions, can be easily written in terms of the Laplace transform. However, it is not possible to obtain the inverse Laplace transform in a closed analytical form in the present case. Sharma and Tewary (1983) have used the Tricomi method (see, for example, Sneddon, 1972) to obtain the solution in a semi-analytic form. Sharma *et al.* (1981) have given an expression for PVD which is valid at small times. In this limit ($z \to 0$), the PVD is given by

$$\Delta V_1(z) = -Az (z \ll 1/\xi \ll 1) \tag{151}$$

where

$$A = \frac{N_0}{J_g} \frac{C_e(l\sqrt{\xi} + 1)(j + 1)\exp(-C_e W_e)}{(j\sqrt{\xi} + 1)} \tag{152}$$

$$l = L_e/L_b$$

and J_g is given by Eq. (62).

Equation (151) is convenient for a qualitative understanding of the effect of p–n coupling on PVD. First, it may be remarked that the decay rate A given by Eq. (152) does not really depend upon N_0 since J_g is proportional to N_0 [see Eq. (62)].

The decay rate A in practical units is shown in Fig. 17 as a function of α for different values of η and S_e. The calculations refer to a n^+–p solar cell used by Fossum *et al.* (1979). The material parameters of this cell are as follows: emitter, $d_e = 0.1\ \mu m$, $\tau_e = 1$ nsec, $L_e = 0.3\ \mu m$ and $J_{e0} = 18.6 \times 10^{-13}$ A/cm^2; base, $\tau_b = 4.1\ \mu$sec, $L_b = 80\ \mu m$ and $J_{b0} = 6.3 \times 10^{-14}$ A/cm^2. It may be noted that in this cell $j \ll 1$ which shows a substantial band-gap shrinkage.

The surface parameters of the emitter, namely η and S_e, affect the decay rate only through J_g and J_{e0}. In fact the dependence of PVD on η comes only through the steady-state ECP. We observe from Fig. 17 that for low values of α, A is quite sensitive to S_e as well as η. This is because J_g decreases as α

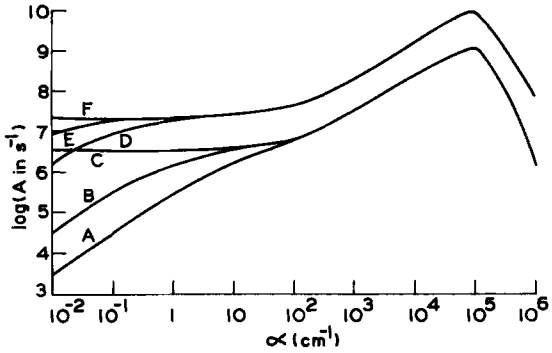

FIG. 17. Variation of decay rate A of open-circuit photovoltage at $t = 0$ as a function of the absorption coefficient α of light. For curves A, B, and C, $S = 10^4$ cm/sec and $\eta = 0.1, 0.01$, and 0, respectively. For curves D, E, and F, $S = 10^7$ cm/sec and $\eta = 0.1, 0.01$, and 0, respectively. Add 13.2 to all numbers on the y axis.

decreases but the absorption at the surface characterized by η does not change. Hence the relative contribution of surface absorption increases.

For very large values of α ($\gg 1/d_e$) the front surface and the emitter again makes a significant contribution because more light is absorbed in the emitter. In this case the surface recombination dominates over surface absorption and therefore A is not sensitive to η for large α. Another interesting feature of Fig. 17 is the existence of a maximum which occurs at approximately $\alpha = 1/d_e$. This arises because of the presence of the $\alpha \exp(-\alpha d_e)$ term on the right-hand side of Eq. (151) (since $C_e = \alpha L_e$). The maximum is not exactly at $\alpha = 1/d_e$ because of the dependence of J_g on α.

More detailed FCVD curves as calculated by Sharma and Tewary (1983) have been shown in Figs. 18–21. Figure 18 shows, as in the case of FCVD discussed in Section IV.C, that the effect of p–n coupling is more pronounced for smaller j (larger a) and larger ξ. Figure 19 gives the effect of η and α on PVD. This figure also gives the corresponding result obtained by using Jain's (1981) theory, i.e., Eq. (87). The effect of η is more significant in the initial stages of the decay, which has been discussed earlier in this section. The main features of the spectral dependence of PVD, i.e., the dependence on α as observed from Fig. 19, are as follows:

1. The effect of p–n coupling is more significant at low values of z. The slope of the linear region in the PVD curve for large z is not affected by p–n coupling. This is similar to FCVD discussed in Section IV.C.

2. The decay rate is faster for large α in the initial stages (low z). This is similar to the case of PVD without p–n coupling as discussed in Section III.B. It is physically expected because the slope of ECP at the junction in the base in

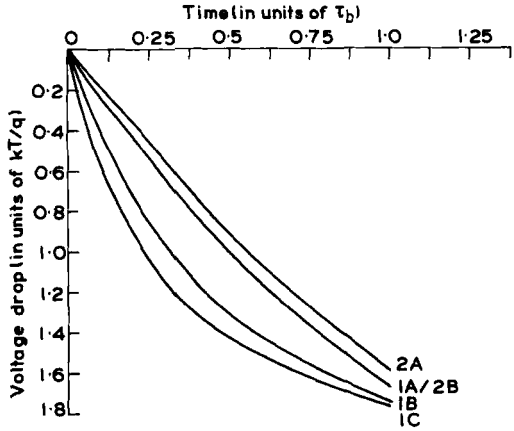

FIG. 18. Effect of relative dark saturation current j (curve 1) and relative minority-carrier lifetime $\xi = \tau_b/\tau_e$ (curve 2) on PVD. For curve 1, $\xi = 1000$ and $j = 0.1$, 5, and 10 for A, B, and C, respectively. For curve 2, $j = 0.1$ and $\xi = 100$ and 1000 for A and B, respectively. For all these curves $\alpha = 10^3$ cm^{-1}, $\eta = 0.01$, $S = 10^3$ cm/sec, and $d = 0.1$ μm.

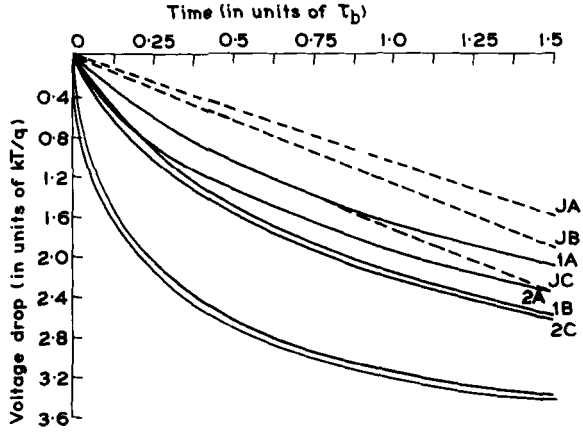

FIG. 19. Effect of the absorption coefficient of light (α) and surface generation coefficient (η) on PVD for $j = 30$, $\tau_e/\tau_b = 0.003$, $d = 0.1$ μm, and $S = 10^4$ cm/sec. Curves 1 and 2 are for $\eta = 0$ and 0.01, respectively; A, B, and C denote the curves for $\alpha = 10$, 10^2, and 10^3 cm^{-1}, respectively. Curves labeled J are obtained by using Jain's theory (in which p–n coupling is neglected) with A, B, and C referring to values of α as above.

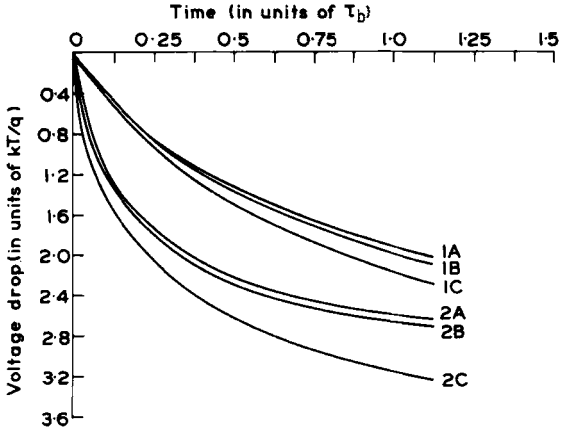

FIG. 20. Effect of surface recombination velocity (S) on PVD. Curves 1 and 2 are for $\alpha = 10^2$ cm^{-1} and 10^3 cm^{-1}, respectively; A, B, and C denote the curves for $S = 10$ cm/sec, 10^2 cm/sec and 10^3 cm/sec, respectively. For all these curves $\eta = 0$, $\tau_e/\tau_b = 0.003$, $j = 30$, and $d = 0.1$ μm.

steady state increases as α increases. This results in a faster diffusive loss of excess carriers at the junction when the decay starts. It may also be noted that, as in the case of PVD without p–n coupling (Jain, 1981), the PVD rate becomes insensitive to α for very large and very small α.

3. The effect of p–n coupling becomes more significant for larger values of α. This, as discussed earlier in this section for low values of z, is due to the fact that more light is absorbed in the emitter.

The effect of S_e on PVD is shown in Fig. 20. It is qualitatively similar to that at low values of z which has been discussed earlier. The effect of the thickness of the emitter d_e on PVD is shown in Fig. 21. We see from this figure that this effect is more for larger values of d_e, which is physically expected since a thicker emitter would absorb more light and hence would store more excess carriers. This effect is more significant for smaller values of j since, as discussed earlier, the effect of p–n coupling itself increases as j decreases.

Sharma and Tewary (1983) have also tried to fit their theoretical PVD curve with the experimental results of Madan and Tewary (1983). However, because of a large number of parameters involved in the theory, a unique set of values of these parameters could not be obtained. It would be interesting to have more detailed experimental results for PVD in a solar cell. If some of the parameters are known by independent measurements it should be possible to estimate τ_e and τ_b by fitting the theoretical and experimental results.

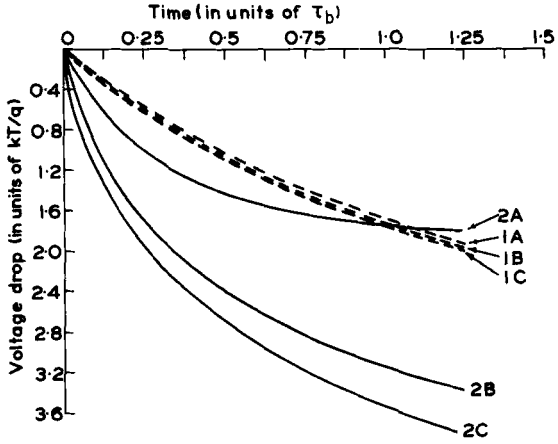

FIG. 21. Effect of diffused layer thickness (d) on PVD. Curves 1 and 2 are for $j = 0.1$ and 10, respectively; A, B, and C denote the curves for $d = 0.1$ μm and 0.3 μm, respectively. For all these curves $S = 10^3$ cm/sec, $\eta = 0.01$, $\tau_e/\tau_b = 0.001$, and $\alpha = 10^3$ cm^{-1}.

V. Quasi-static Emitter Approximation and Its Applications in Solving Coupled Diffusion Equations for OCVD

In the previous chapter we saw that the effect of p–n coupling on OCVD can be quite significant in certain cases. In general the mathematical problem of solving the coupled diffusion equations is quite complicated. An analytical solution, i.e., the North's expression could indeed be obtained for FCVD in thick diodes but in a general case of practical interest, one has to resort to numerical or semianalytical treatment as in the case of PVD in Section IV.D.

In this section, we shall describe the so-called quasi-static emitter (QSE) approximation which was proposed by Jain and Muralidharan (1981) and which can be used for solving the coupled diffusion equations. The QSE approximation effectively decouples the two diffusion equations by modifying the boundary condition at the junction. With the help of QSE approximation, it would suffice to solve the diffusion equation in the base while the effect of emitter is approximately included in terms of a modified boundary condition. The QSE approximation has been shown to be quite accurate for $t \gg \tau_e$.

The QSE approximation has been found to be quite accurate except for very small times (of the order of τ_e). For the purpose of determining τ_b and the band-gap shrinkage the region of time $\tau_e \ll t \lesssim \tau_b$ is of considerable practical interest. In this region the QSE approximation has been found to be extremely

useful. The QSE approximation is of course valid even for larger times $t \gg \tau_b$ but then the effect of p–n coupling itself becomes insignificant.

In this section we shall first illustrate the QSE approximation by applying it to calculate FCVD in thick diodes for which the exact result, i.e., the North's expression, is available as described in Section IV.B. We shall then use the QSE approximation to calculate FCVD in a thick diode containing a constant drift field in the base and PVD in a solar cell with arbitrary thickness with and without a constant drift field in the base. In all these cases the effect of p–n coupling is included through the QSE approximation while still neglecting the high injection effects.

A. QSE Approximation

The main assumption in the quasi-static approximation is that the shape of the ECP does not change during decay. We make this assumption for the emitter only and not for the base. Thus we write the following for the time-dependent ECP in the emitter:

$$q_e(X_e, z) = q_{es}(X_e) f_1(z) \tag{153}$$

where $q_{es}(X_e)$ is the ECP in the steady state and the function $f_1(z)$ is to be determined. As we shall see in this and the following subsections, use of Eq. (153) in the zero-current condition at the junction decouples the diffusion equations, resulting into a considerable simplification.

It is tempting to try a similar quasi-static approximation in the base as well. Such an attempt was made by Lindholm and Sah (1976). However, detailed calculations of Jain and Muralidharan (1981) show that, except for a short duration of time, the ECP in the emitter retains its steady-state shape. On the other hand, the shape of ECP in the base deteriorates very fast after the decay starts. The quasi-static approximation is therefore not valid in the base.

We now illustrate the use of QSE approximation for calculating FCVD in a thick diode. The exact solution of this problem has already been given in Section IV.B. Using Eq. (153) in the zero-current condition given by Eq. (133) we obtain

$$\frac{L_b}{\tau_b}\left[\frac{\partial q_b(X_b, z)}{\partial X_b}\right]_{X_b=0} = \frac{L_e}{\tau_e}\left[\frac{\partial q_{es}(X_e)}{\partial X_e}\right]_{X_e=0} f_1(z) \tag{154}$$

The function $f_1(z)$ in fact gives the voltage decay. This can be seen by using the voltage condition as given by Eq. (132) in Eq. (153) which gives the following result:

$$f_1(z) = \exp[\Delta V_1(z)] \tag{155}$$

where we have used the inequality (79).

The coefficient of $f_1(z)$ on the right-hand side of Eq. (154) is the emitter current at the junction in the steady state as given by Eq. (19) for $E_{ej} = 0$. Using Eqs. (41) and (29), we obtain from Eq. (154)

$$\frac{L_b}{\tau_b}\left[\frac{\partial q_b(X_b, z)}{\partial X_b}\right]_{X_b=0} = \frac{J_{e0} q_{bj}}{q_{b0}}$$

or

$$\left[\frac{\partial q_b(X_b, z)}{\partial X_b}\right]_{X_b=0} = a q_{bj} \tag{156}$$

where $a = 1/j$ as given by Eq. (141).

We see that the QSE approximation used along with the current and the voltage conditions has yielded a relation between the derivative and the height of the ECP in the base at the junction. The effect of emitter or the p–n coupling is represented by the parameter a. Equation (156) can be prescribed as the boundary condition at the junction. It would thus suffice to solve the diffusion equation in the base subject to the boundary condition at the junction as given by Eq. (156) and the appropriate boundary condition at the back surface of the base.

The solution of Eq. 125, i.e., the diffusion equation in the base of the diode can now be easily obtained by using the Laplace transform method. The boundary conditions are as given by Eq. (127) for $q_b(X_b, z)$ and Eq. (156) with the initial condition specified by Eqs. (131) and (37). The result is

$$\exp[\Delta V_1(z)] = \frac{e^{-z}}{1-a}[S(z) - aS(a^2 z)] \tag{157}$$

We note that Eq. (157) is identical to Eq. (142), which was obtained by approximating Eq. (134). As we have already discussed in Section IV.B (see also Madan and Tewary, 1985), this approximation is very good for $t \gg \tau_e$. Unless our interest is particularly in the determination of τ_e and other characteristics of the emitter, the QSE approximation should prove to be adequate.

As shown by Jain and Muralidharan (1981) and Jain and Ray (1983a), the QSE approximation is valid, except at short times of the order of τ_e, provided the following two conditions are satisfied:

$$1. \qquad \xi \gg 1 \tag{158}$$

$$2. \qquad \tau_{eff} \gg \tau_e \tag{159}$$

where τ_{eff} is the effective lifetime of excess carriers as determined from the slope of the linear region in the OCVD curve [see Section III.C, Eq. (103)].

B. Effect of Drift Field on FCVD in a Thick Diode

This problem has been solved by Jain and Ray (1983a) using the QSE approximation which gives the results in a closed analytical form. The time-dependent diffusion equation for the excess carriers in the base is the same as Eq. (75) which is rewritten below:

$$\frac{\partial^2 q_b}{\partial X_b^2} + 2F_b \frac{\partial q_b}{\partial X_b} - q_b = \frac{\partial q_b}{\partial z} \tag{160}$$

The explicit dependence of q_b on X_b and z has not been shown for notational brevity. The boundary condition at the back of the base is given by Eq. (127). We need to specify the current and the voltage conditions at the junction as given by Eqs. (21) and (29), respectively. Using the QSE approximation (Jain and Ray, 1983a) and following the steps leading to Eq. (156) we obtain the following boundary condition at $X_b = 0$:

$$\partial q_b / \partial X_b + 2F_b q_b = a q_b \tag{161}$$

In addition, we have to specify the initial condition as given by Eq. (131) and Eq. (48). Equation (160) can now be easily solved by using the Laplace transform method. The final result is

$$\exp[\Delta V_1(z)] = \frac{e^{-z_1}}{1 - a_1}[S(z_1) - a_1 S(a_1^2 z_1)] \tag{162}$$

where

$$a_1 = (a - F_b)/\sqrt{(1 + F_b^2)} \tag{163}$$

and

$$z_1 = (1 + F_b^2)z \tag{164}$$

Equation (162) is similar to Eq. (157) with a and z replaced by a_1 and z_1, respectively. This similarity is not surprising because, as shown in Section II, the solution of Eq. (160) is related to the solution of Eq. (153) through a simple transformation.

The effect of the emitter on FCVD as given by Eq. (162) is represented by the coupling parameter a_1. This parameter depends upon the drift field in the emitter F_e, τ_e, and band-gap shrinkage ΔE_g. In general all these quantities, i.e., F_e, τ_e, and ΔE_g are not constant throughout the emitter. Jain and Ray (1983a) assumed them to be constant, having appropriate effective values which determine J_{e0} and hence the coupling parameter. In terms of the effective values of F_e, τ_e, and ΔE_g, J_{e0} is given by

$$J_{e0} = J'_{e0}[F_{1e}\coth(F_{1e}W_e) - F_e]\exp(\Delta F_g/kT) \tag{165}$$

where J_{e0} is the saturation current for $F_e = 0$, $\Delta E_g = 0$, and $W_e = \infty$ and

$$F_{1e} = (1 + F_e^2)^{1/2} \tag{166}$$

As given in Section IV.C, the value of a and hence J_{e0} can be estimated from the FCVD data. Equation (165) can then be used to estimate ΔE_g since F_e can be estimated from the known doping profile in the emitter.

We shall now discuss the effect of drift field in the emitter on FCVD. For simplicity we assume that $\Delta E_g = 0$ and $W_e = \infty$. This gives

$$a = a_0[F_{1e} - F_e] \tag{167}$$

where a_0 is the value of a for $F_e = 0$. We see from Eq. (167) that for retarding fields ($F_e > 0$), a will decrease as F_e increases. The effect of p–n coupling will therefore decreases as F_e increases. In the limit $F_e = \infty$, $a = 0$, the diode will behave like a base-dominated diode. This is physically expected because a retarding field drives the carrier toward the junction. Hence the injection efficiency of the emitter increases with increasing F_e. It becomes unity for $F_e = \infty$, i.e., the diode becomes a base-dominated diode.

On the other hand, an accelerating field ($F_e < 0$) drives the carriers away from the junction. We expect physically therefore that an accelerating field will accelerate the decay. Due to a faster depletion of carriers at the function in the emitter, the base has to provide more carriers to the junction to satisfy the voltage condition. The strength of p–n coupling will therefore increase as the accelerating field increases. This is predicted mathematically by Eq. (167) which shows that, for $F_e < 0$, a increases as the magnitude of F_e increases.

The effect of drift field in the base is to replace a and z by a_1 and z_1 in accordance with Eqs. (163) and (164), respectively. From the similarity between Eqs. (163) and (142) we expect that $V_1(z)$ will become linear in z for large z and the slope of the linear region will be $(1 + F_b^2)$. The effective lifetime in the base, as determined from this slope, is therefore given by

$$\frac{1}{\tau_{\text{eff}}} = \frac{1}{\tau_b}(1 + F_b^2) \tag{168}$$

We infer therefore, as physically expected, that acceleration drift fields will accelerate the decay. In the limit $|F_b| = \infty$, τ_{eff} as given by Eq. (168) becomes zero. However, in this limit the inequality (158) will be violated and hence the QSE approximation will not be valid. Further, we see from Eq. (163) that a_1 will increase as the magnitude of F_b increases so that the strength of p–n coupling will also increase for acceleration drift fields. The increased p–n coupling will accelerate the decay in the initial stages.

Figures 22 and 23 show the calculated FCVD curves for different magnitudes of accelerating as well as retarding drift fields. The effect of accelerating drift fields has already been discussed. The effect of retarding drift

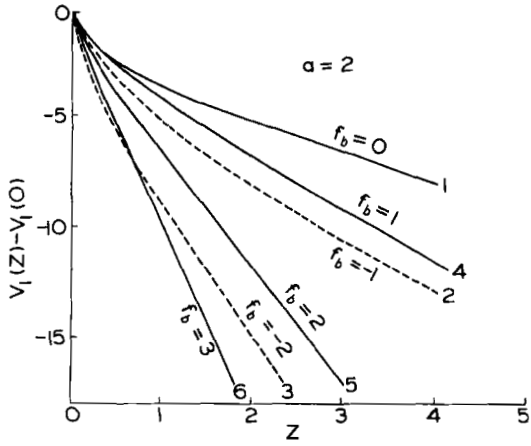

FIG. 22. FCVD plots for several values of accelerating (negative F_b) and retarding (positive F_b) drift fields in the base. The parameter a is equal to 2 for all the plots.

fields, as can be seen from Fig. 22, is also to accelerate the decay. This apparently inconsistent effect can be understood as follows.

We notice from Eq. (163) that for large retarding drift fields ($F_b > 0$), a_1, the effective coupling parameter, becomes negative. It can be shown (Jain and Ray, 1983a) that, even for negative values of a_1, the function on the right-hand side of Eq. (162) has a linear dependence on z_1 for large z_1. The FCVD in this region of time is given by the following expression which is valid for

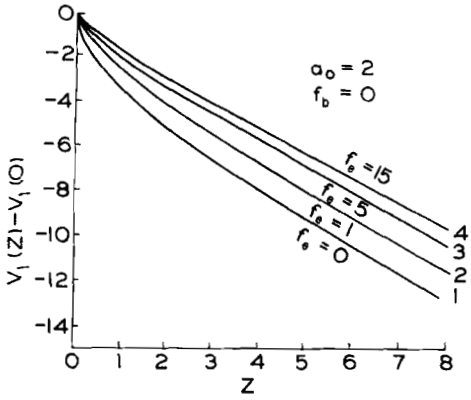

FIG. 23. FCVD plots for several values of retarding drift fields in the emitter for a diode in which the emitter is not heavily doped and there is no drift field in the base. The parameter a_0 [see Eq. (167)] has been taken as 2 for all the plots.

$F_b > a > 0$:

$$\Delta V_1(z) = -(1 - a_1^2)(1 + F_b^2)z + \ln\left(\frac{2|a_1|}{1 + |a_1|}\right) \tag{169}$$

The effective lifetime as defined in terms of the slope of this linear region is then given by

$$\frac{1}{\tau_{eff}} = \frac{1}{\tau_b}[(1 + F_b^2) - (a - F_b)^2] \qquad (F_b > a > 0) \tag{170}$$

We see from Eq. (170) that, since $F_b > a > 0$, by hypothesis $\tau_{eff} < \tau_b$. This explains how the voltage decay becomes faster because of a strong retarding field in the base. In fact this case is particularly interesting because here the p–n coupling has made a qualitative difference in FCVD. That this result arises from p–n coupling is clear from Eq. (170) since if we put $a = 0$ in this equation, τ_{eff} becomes equal to τ_b. This is consistent with Eq. (119), which shows that in the case of a strong retarding drift field in a base-dominated diode, $\tau_{eff} = \tau_b$ and is independent of F_b as well as W_b.

In the case of weak retarding drift fields ($0 < F_b < a$), we see from Eq. (163) that as F_b increases from zero, a_1 decreases. This reduces the strength of the p–n coupling. When F_b becomes equal to a, $a_1 = 0$ and the p–n coupling becomes zero.

C. FCVD in Thin Base Diodes with Constant Drift Field

In this section we shall mainly report the results of Ray *et al.* (1982). The diffusion equation for this case is the same as Eq. (160). The QSE boundary condition at the junction that accounts for the p–n coupling is as given by Eq. (161). The boundary condition at the back of the base is as given by Eq. (106). The steady-state profile required for the initial condition, i.e., Eq. (33) is obtained from Eq. (46) using the transformation given by Eq. (48).

The diffusion equation in the base, subject to the boundary conditions mentioned above, is solved by the usual method of expansion in terms of orthogonal functions. As in Sections III.C and D, the following expression for FCVD can be easily derived (Ray *et al.*, 1982):

$$\exp[\Delta V_1(z)] = \sum_r A_r \exp(-\varepsilon_r^2 z) \tag{171}$$

where

$$\varepsilon_r^2 = 1 + F_b^2 + \mu_r^2 \tag{172}$$

and μ_r are obtained as the roots of the following equation:

$$(S_b^* + a)\mu_r - [\mu_r^2 + (F_b - a)(S_b^* + F_b)]\tan(\mu_r W_b) = 0 \tag{173}$$

As in Section III.C or D, the effective lifetime is obtained in terms of the slope of the linear region of the FCVD curve. In the present case it is given by

$$\frac{1}{\tau_{\text{eff}}} = \frac{1}{\tau_b}(1 + F_b^2 + \mu_0^2) \tag{174}$$

where μ_0 is the smallest real or imaginary root of Eq. (173). As mentioned in Sections III.C and D, μ_r do not depend upon the steady-state ECP. The coefficients A_r are obtained by the steady-state ECP.

The FCVD curves for different positive and negative values of F_b have been shown in Fig. 24. For all these curves the value of a is taken to be unity and $S_b^* = \infty$. We see from this figure that the voltage decay becomes faster for retarding as well as accelerating fields. This is similar to the result obtained in the preceding section. As mentioned in that section, the retarding field makes the decay faster because of the p–n coupling.

The effect of SRV at the back surface of the base (i.e., at the low–high junction) on FCVD is shown in Fig. 25. For these calculations, the values of W_b, a, and F_b are taken to be unity. It is found that FCVD is not sensitive to S_b^* for $S_b^* > 100$ for $W_b = 1$. This $S_b^* = 100$ almost corresponds to the limiting case of an ohmic contact. In general, as found in Section III.C without p–n coupling, the voltage decay becomes faster as S_b^* increases. This is physically expected because an increase in S_b^* for small values of W_b would result in a faster removal of carriers from the junction.

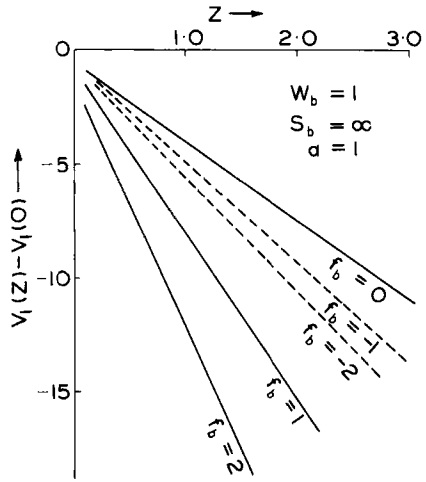

FIG. 24. The reduced voltage $V_1(z) - V_1(0)$ versus reduced time for various values of the base drift fields.

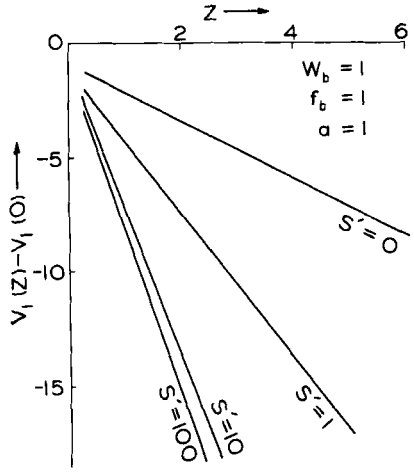

FIG. 25. The reduced voltage $V_1(z) - V_1(0)$ versus reduced time $z = t/\tau_b$ for different values of reduced surface recombination velocity at the base $S_b^* = S_b L_b/D_b$.

Ray *et al.* (1982) have also reported their experimental results on FCVD in the n^+–p–p^+ silicon varactor diode. Their observed FCVD curve is shown here in Fig. 26. We see from this figure that the linear region starts very soon and extends up to about 1 μsec. The curvature after 1 μsec is attributed to the space-charge layer.

The diode used in the experiments was quite thin (W_b was small). Hence the series in Eq. (171) is very rapidly convergent. Within a short time, the first term

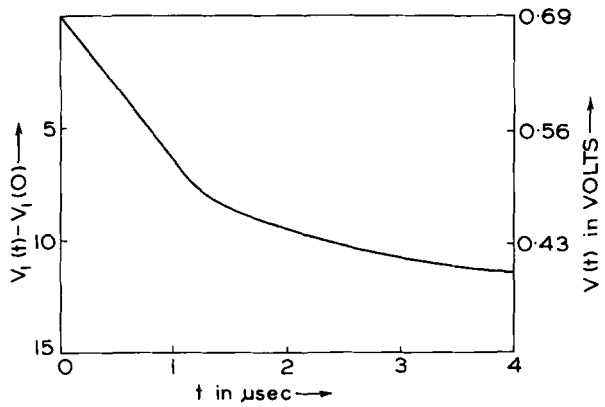

FIG. 26. The observed voltage decay curve for a diode.

in this series starts dominating over higher terms. This explains the early onset of the linear region in the FCVD curve. The effective lifetime, as determined from the slope of this linear region, comes out to be 0.16 μsec.

From the known doping profile in the base, Ray *et al.* (1982) estimated $S_b^* = 0$ (showing a very "good" BSF diode) and drift field E_b to be 36 V/cm. They estimated the value of a to be approximately unity by using the dark I–V characteristics of the diode. Finally, the value of τ_b, as determined from the FCVD data, is found to be 0.5 μsec with $F_b = 3$.

D. PVD in Solar Cells

In this section we shall use the QSE approximation to calculate PVD in thick as well as thin solar cells including the effect of p–n coupling. For thick solar cells, the effect of p–n coupling on PVD has already been discussed in Section IV.D without using the QSE approximation. The advantage of QSE approximation is that it yields the result in a closed analytical form as obtained by Jain and Ray (1983b). The effect of drift field is neglected.

First we consider a thick base solar cell. The diffusion equation for the base is same as Eq. (75) for $F_b = 0$ [or Eq. (125)] and only monochromatic illumination is considered. The boundary condition at the back is as given by Eq. (127). The initial condition is prescribed by Eq. (131) with the steady-state ECP given by Eq. (64). It may be remarked that this expression for steady-state ECP does not include the contribution of the emitter. However, the nature of the steady-state ECP affects PVD only in the early stages of decay for which the QSE approximation is not valid any way. The effect of p–n coupling on PVD at low times has already been discussed in Section IV.D.

The boundary condition at the junction is derived by using the QSE approximation (Jain and Ray, 1983b) and is given below:

$$\left[\frac{\partial q_b(X_b)z}{\partial X_b}\right]_{X_b=0} = aq_b(0, z) \tag{175}$$

The solution of the diffusion subject to aforementioned boundary and initial conditions can be obtained by the Laplace transform method. The resulting expression for PVD (Jain and Ray, 1983b) is as follows

$$\exp[\Delta V_1(z)] = \frac{C_b e^{-z}}{(1 - C_b)(a - 1)}[S(z) - aS(a^2 z)] - \frac{e^{-z}}{(1 - C_b)(a - C_b)}[C_b S(C_b^2 z) - aS(a^2 z)] \tag{176}$$

It has been verified by actual numerical calculations that, as mentioned earlier in this section, the final result for $t \gg \tau_e$ (or $z \gg 1/\xi$) is not sensitive to whether the steady-state ECP included the effect of the emitter or not.

The PVD curves as calculated from Eq. (176) (Jain and Ray, 1983b; also see Mallenson and Landsberg, 1977) have been shown in Fig. 27 for $a = 0$ and 2 and for $C_b = 0.5$. The figure also shows the FCVD curve for $a = 2$. The qualitative nature of the effect of p–n coupling on PVD as indicated by Fig. 27 is of course the same as discussed in Section IV.D.

An expression for PVD which includes the effect of p–n coupling in thin solar cells can also be derived quite easily by using the QSE approximation. We consider a solar cell having BSF in the base but no drift field. The boundary condition at the back of the base is given by Eq. (13). The steady-state ECP is taken to be that given by Eq. (65) or Eq. (69) depending upon the value of S_b^*. The boundary condition at the junction is the same as prescribed by Eq. (175), which was obtained by using the QSE approximation. The expression for PVD as obtained by the standard method of expansion in terms of orthogonal functions is given below:

$$\exp[\Delta V_1(z)] = \sum_r A_r \exp(-\varepsilon_r^2 z) \tag{177}$$

where, as in the earlier cases, A_r are obtained by using the steady-state ECP,

$$\varepsilon_r^2 = 1 + \mu_r^2 \tag{178}$$

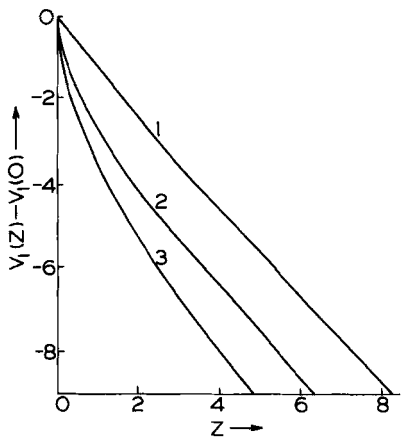

FIG. 27. PVD for a solar cell with base thickness W_b. Curve 1 corresponds to a base-dominated cell ($a = 0$) and curve 2 is for the coupling parameter $a = 2$. The value of $C(= \alpha L_b)$ for the curves 1 and 2 is 0.5. Curve 3 is the FCVD plot for $a = 2$.

and μ_r are the roots of the following equation:

$$(S_b^* + a)\mu_r - (\mu_r^2 - aS_b^*)\tan(\mu_r W_b) = 0 \tag{179}$$

The series on the right-hand side of Eq. (177) is rapidly convergent for large z and low W_b. The effective lifetime determined as in Eq. (103) or Eq. (104) is written in the following form

$$\frac{1}{\tau_{eff}} = \frac{1}{\tau_b} + \frac{1}{\tau_1} \tag{180}$$

where

$$\tau_1 = \tau_b/\mu_0^2 \tag{181}$$

and μ_0 is the leading root of Eq. (179).

The parameter τ_1 in fact does not explicitly depend on τ_b (Jain and Ray, 1983b). This is because μ_0 is proportional to $1/W_b$ and therefore to L_b where L_b, the diffusion length, is $(D_b\tau_b)^{1/2}$. A weak implicit dependence of τ_1 and τ_b comes through the dependence of μ_0 on parameter a (since the saturation currents depend upon the diffusion lengths). Thus, for all practical purposes, τ_1 can be treated as independent of τ_b.

The effect of p–n coupling as well as finite thickness of the base of the solar cell are included in τ_1. The calculated values of τ_1 in a real solar cell (Jain and Ray, 1983b) are shown in Fig. 28 as a function of SRV, for different values of J_{e0} and W_b. In these calculations $D_b = 13$ cm^2/sec and $q_{b0} = 0.82 \times 10^{-14}$ C/cm^3. These values correspond to a n-type base of resistivity 1 Ω-cm.

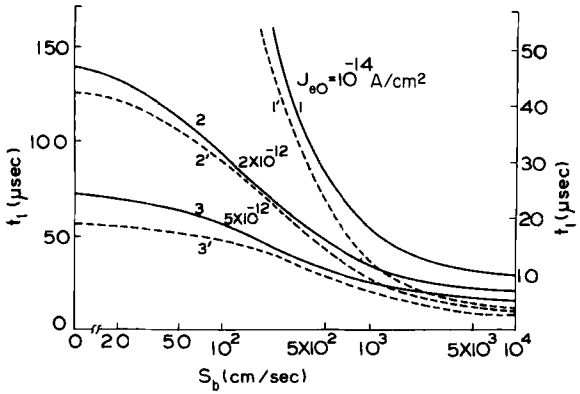

FIG. 28. Characteristic decay time constant t_1 for 1 Ω-cm n-type base solar cell as a function of S_b for different values of J_{e0}. The solid curves correspond to $d_b = 300$ μm and the dotted ones are for $d_b = 100$ μm. The y-axis scales for the solid and dotted curves are, respectively, given by the left- and right-hand side of the figure.

For an ideal BSF solar cell ($S_b^* = 0$), it can be easily verified that if $a = 0$ (no p–n coupling) $\mu_0 = 0$ and $\tau_1 \simeq \infty$ so that $\tau_{eff} = \tau_b$. This is the same case as given by Eq. (112). We see that in the absence of p–n coupling, the PVD rate is independent of the thickness of the base.

In a solar cell in which a is quite large due to band-gap shrinkage in the emitter, the effect of p–n coupling will be significant. It will make the voltage decay faster. We see from Fig. 28 that for small values of S_b^*, τ_1 decreases rapidly as J_{e0} (and hence a) increases. In a typical n^+–p–p^+ solar cell where $J_{e0} = 2 \times 10^{-12}$ A/cm^2 (including the effect of band-gap shrinkage), $d_b = W_b L_b = 300$ μm, and $S_b^* = 0$, we find that $\tau_1 = 138$ μsec (Rose, 1981; Weaver, 1981). For this solar cell $\tau_b = 105$ μsec. The value of τ_{eff} comes out to be 63 μsec. Thus we see that in such cases the slope of the linear region in the PVD curve will provide a poor estimate of τ_b.

It is interesting to see that the p–n coupling makes the PVD rate quite sensitive to the thickness of the base. This effect is even stronger for larger values of $\xi (= \tau_b/\tau_e)$. Jain and Ray (1983b) find that in certain cases p–n coupling can reduce the effective lifetime by as much as 70%.

In a conventional solar cell ($S_b^* = \infty$), Jain and Ray find that for small d_b, τ_{eff} is not very sensitive to J_{e0}. This and the above result can be physically understood as follows.

During decay, the ECC near the junction in the base decays by the following three processes: (1) recombination, (2) reverse flow in the emitter due to p–n coupling, and (3) diffusion away from the junction toward the back contact.

In a conventional solar cell ($S_b^* = \infty$), the ECC at the back is always zero. If the thickness of the base is small the ECP becomes very steep. In this case the diffusive loss of excess carriers becomes very strong and the process (3) dominates. The effect of p–n coupling is relatively insignificant, i.e., τ_{eff} is not sensitive to J_{e0}. In an ideal BSF cell $S_b^* = 0$. The proximity of back contact to the junction (i.e., small d_b) makes the ECP quite flat, which reduces the contribution of the process (3). In such cases the process (2) dominates, i.e., the effect of p–n coupling becomes very significant.

VI. High Injection Effects on FCVD

In this section we shall discuss the effect of high injection on FCVD. Although we shall mostly refer to FCVD, the basic ideas and the physical processes which we shall discuss will also be relevant to PVD.

We define a semiconductor to be in a high injection state when the concentration of injected carriers, i.e., the ECC is of the order of, or exceeds,

the concentration of majority carriers at thermal equilibrium in the semiconductor. In a p–n diode or a solar cell the emitter is much more heavily doped than the base. The base therefore reaches the high injection state at a much lower level of injection than the emitter.

In a diode or a solar cell when the emitter also reaches the high injection state, then the junction potential becomes comparable to the diffusion potential of the device. The maximum value of the junction potential in a device is of course equal to its diffusion potential as can be seen from Fletcher voltage conditions given by Eqs. (22) and (23). The proximity of the junction potential to the diffusion potential of the device is, therefore, a measure of the level of injection in the device.

In the past few years a considerable amount of experimental work has been done on high injection effects on OCVD (see, for example, Bassett *et al.*, 1973; Derdouri *et al.*, 1980; Cooper, 1983; also the review by Green, 1984, which also gives other references). Some of these results are very fascinating. A suitable theoretical explanation of these effects is not yet available in the literature. In this section we shall attempt to identify the physical processes which might be responsible for the observed high injection effects on OCVD. Based upon these processes, we shall present a theoretical analysis of the experimental results on high injection FCVD. A theory of FCVD at high injection would be mathematically rather complicated because of the nonlinearity of high injection effects. In this section therefore, we shall use reasonable approximations including the QSE approximation to analyze the high injection effects on FCVD.

A. Nature of High Injection Effects on OCVD

First we summarize the nature of experimentally observed high injection effects on PVD and FCVD curves.

1. In some devices the slope of the FCVD as well as PVD curves is small in the beginning and increases after some time. (Bassett *et al.*, 1973; Green, 1984). An example of this behavior is given in Fig. 29. This figure shows some PVD curves for a 10 Ω-cm base-resistivity n^+–p solar cell which have been observed at the Solid State Physics Laboratory (SSPL), Delhi, by S. C. Jain, U. C. Ray, and their colleagues (private communication).

2. In some cases of FCVD it is found that the voltage drops rapidly in the beginning, then remains constant for a while and then finally decays to zero. The region of the FCVD curve in which the voltage remains constant (almost zero slope) will be referred to as the "plateau" in the FCVD curve. In some cases, after the initial drop, the voltage rises for a while and then decays to 0.

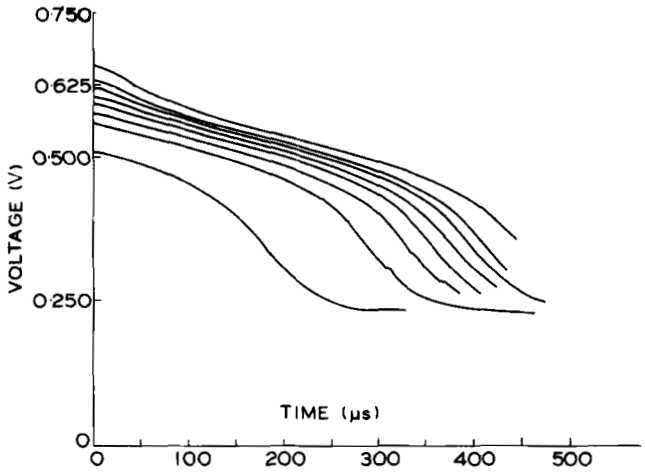

FIG. 29. High injection PVD in a silicon solar cell with 10 Ω-cm resistivity base. These experimental results were obtained by D. K. Bhattacharya, S. C. Jain, R. Muralidharan, and U. C. Ray at SSPL, Delhi (private communication).

The rise and the fall in the voltage decay curve is referred to as the "hump" in the FCVD curve, in contrast to plateau mentioned earlier.

The hump/plateau can be clearly seen in the experimental FCVD curves published by Derdouri *et al.* (1980) and Cooper (1983). The existence of the hump and the plateau in FCVD curves has been further confirmed by the detailed experimental investigation on FCVD carried out at SSPL, Delhi by S. C. Jain, U. C. Ray, and their colleagues (private communication). Some of their results are shown in Fig. 30. This figure shows FCVD curves in a p–n diode of 1000 Ω-cm resistivity base at different levels of injection. The fast drop in the beginning of the FCVD curves followed by a hump or a plateau can be clearly seen in Fig. 30. If the injection level is not high enough, the plateau in the FCVD curve is replaced by a regin of small slope. As the injection level rises this region becomes a plateau and then a hump. It may be remarked that a plateau in a FCVD curve can be taken to be a special case of a hump i.e., a region in which the voltage could not rise enough to become a hump.

It appears from the very detailed and extensive work at SSPL, Delhi that the hump/plateau in FCVD curves is observed only in p–i–n diodes or n^+–p–p^+ (or p^+–n–n^+) devices, i.e., those containing BSF. It seems therefore that the existence of two junctions as in p–i–n diodes or devices with BSF is essential for occurrence of the hump/plateau in the FCVD curves. Moreover, this behavior has been observed only in high-resistivity devices. This is

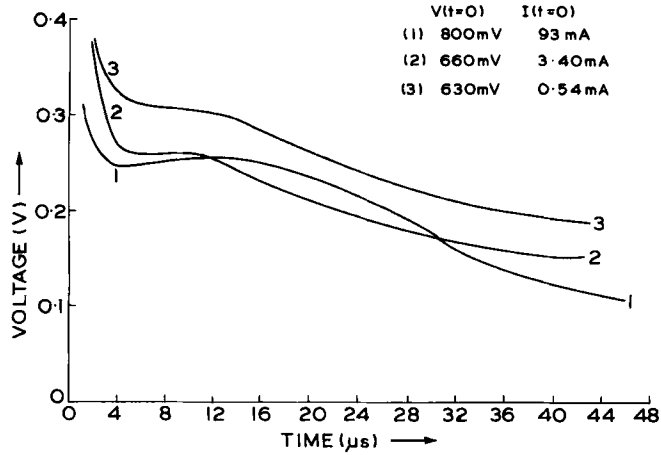

FIG. 30. High injection FCVD in a 1000 Ω-cm resistivity base p–i–n diode. These experimental results were obtained by S. C. Jain, R. Muralidharan, and U. C. Ray at SSPL, Delhi (private communication). Note the formation of the plateau and the hump as the injection level increases.

presumably because the high injection effects would set in at a relatively low level of injection in a high resistivity device as compared to a low resistivity device since the thermal equilibrium value of the carrier concentration is relatively low in a high-resistivity device.

The observations (1) and (2) are inconsistent with each other. In (1) there is a slow decay region in the beginning followed by faster decay of the voltage. In (2) the voltage decays rapidly in the beginning and then either shows a plateau or a hump. Moreover, the nature of high injection effects seems to be quite sensitive to the method of fabricating the devices. In view of various uncertainties and discrepancies in the experimental results, it would be interesting to carry out more detailed and careful measurements on the high injection FCVD and PVD. In FCVD, it would also be necessary to separate out the ohmic drop from any coupling drop by using, for example, the method suggested in Section IV.C.

Theoretically the following three factors would affect the high injection OCVD.

1. Change in Ambipolar Coefficients

As described in Section II.B the coefficients of the ambipolar diffusion equation, i.e., Eq. (1) are functions of ECC and therefore of the level of injection. The dependence of various ambipolar coefficients on the injection

level has been studied by several authors (see, for example, Agarwala and Tewary, 1980).

As shown in Section II.B, all the ambipolar coefficients become constaints in the high injection limit. The high injection limit of ambipolar diffusion coefficient is equal to the harmonic mean of the diffusion coefficients for the two types of carriers [see Eq. (8)]. In general the variation of the ambipolar diffusion coefficient between its low and high injection limit is not large unless the diffusion coefficients for the two types of carriers are drastically different.

The ambipolar mobility decreases as the level of injection increases. It becomes zero in the limit of extreme high injection [see Eq. (9)]. The most important change with the level of injection occurs in the ambipolar life time. As the injection level increases, it increases in general but the actual dependence on the level of injection is quite complicated, as mentioned in Section II.B. According to calculations of Dhariwal *et al.* (1981) the lifetime increases quite substantially as the injection level increases due to saturation of traps. In extreme cases the lifetime may even change by a factor of 5.

However, at extreme high injections, Auger recombination process can decrease the carrier lifetime very substantially. The Auger process makes a significant contribution when the carrier concentration is of the order of 10^{19} cm^{-3} or more. At such high concentrations the diffusion coefficient will also decrease due to carrier–carrier scattering. These processes have obviously not been accounted for in the ambipolar diffusion equation.

It is tempting to explain the initial region of low slope, i.e., observation (1) in the FCVD curve in terms of an increase in the ambipolar life time of excess carriers. However, the aforementioned slope is so small at very high injections that it would require an extremely large increase in the lifetime, viz. by a factor of about 50. The ECC required for such a large increase is not attained in normal experiments. However, at such high concentrations the Auger process becomes significant, which would reduce the excess carrier lifetime.

2. *Change in the Strength of p–n Coupling*

At high injections the strength of p–n coupling increases. This can be easily seen by estimating the value of the coupling parameter a. For this purpose, we use the Fletcher voltage conditions as given by Eqs. (22) and (23). It may be remarked that in this context we should use the Fletcher conditions which give the junction voltage and not the Misawa conditions which give the terminal voltage. Using Eq. (141) for a and the Fletcher conditions, we formally obtain the following expression for a:

$$a_{\text{eff}} = \zeta \sqrt{(D_e \tau_b / D_b \tau_e)} \tag{182}$$

where

$$\zeta = \frac{q_{e0} + q_{b0} \exp[q(V_j - V_D)/kT]}{q_{b0} + q_{e0} \exp[q(V_j - V_D)/kT]} \tag{183}$$

As mentioned earlier the proximity of the junction potential V_j to the diffusion potential V_D is indicative of the state of high injection. The parameter ζ in Eq. (182) can thus be treated as a measure of the dependence of the coupling parameter on the level of injection. For low injections $V_j \ll V_D$ so that $a_{eff} = a$, as defined by Eq. (141).

We assume for the time being that $(D_e\tau_b/D_b\tau_e)$ is independent of the level of injection. We first consider the case when there is no band-gap shrinkage in the emitter and $q_{e0} \ll q_{b0}$. Then, from Eqs. (182) and (183)

$$a_{eff} = a(q_{b0}/q_{e0}) \exp[q(V_j - V_D)/kT] \tag{184}$$

We see that in the high injection limit when $V_j \approx V_D$, the coupling parameter increases by a factor q_{b0}/q_{e0} which is very large. If we include the injection level dependence of D_e, D_b, τ_b, and τ_e there would be no qualitative change in this conclusion. This is because $(D_e\tau_b/D_b\tau_e)$ will have a very weak dependence on the level of injection; it will in fact increase with injection level until the Auger process drastically reduces τ_b without affecting τ_e.

Even with a substantial band-gap shrinkage, in many cases of practical interest, q_{e0} is less than q_{b0} and the above conclusion is still valid. If the gap shrinkage is so large that $q_{e0} \approx q_{b0}$, then as indicated by Eq. (183), ζ and therefore a_{eff} become independent of the level of injection. The extreme case of $q_{e0} \gg q_{b0}$ is not of practical interest.

We conclude therefore that, in general, the strength of the p–n coupling increases at high injections. The effect of p–n coupling, therefore, has to be included in OCVD calculations at high injections, even in base-dominated devices in which p–n coupling is negligible at low injections.

3. *Voltage Boundary Condition at the Junction*

At high injections the Shockley boundary conditions given by Eqs. (28) and (29) are not valid. We have to use Fletcher or Misawa boundary conditions as given by Eqs. (22) and (23) or (25) and (26), respectively. The Shockley boundary conditions are linear in the sense that q_{ej}/q_{bj} is independent of V_j or time. The Fletcher and Misawa conditions are nonlinear. It is normally not possible to obtain a solution of the diffusion equation in a closed analytical form using the nonlinear boundary conditions. In this section we shall discuss only qualitatively the effect of Fletcher and Misawa boundary conditions on FCVD.

First we consider the Fletcher conditions as given by Eqs. (22) and (23). We see from these equations that $q_{ej} = q_{bj} = \infty$ in the limit $V_j = V_D$, which is theoretically the maximum value of V_j. In the extreme high injection case defined by

$$|V_j - V_D| \ll \frac{kT}{q} \tag{185}$$

We obtain the following expression for V_j from Eqs. (22) and (23)

$$V_j = V_D - \frac{kT}{q} \frac{q_{e0} + q_{b0}}{q_{ej}} \tag{186}$$

Equation (186) shows that for large q_{ej}, V_j is not sensitive to q_{ej} and remains close to V_D. Thus we infer that as q_{ej} decays from an almost infinite value to lower but still large values, V_j will not change significantly and remain close to V_D. Thus it would seem to explain the observation 1 given earlier in this section, i.e., the existence of a low slope region in the initial stages of the FCVD region.

More detailed calculations on FCVD using the Fletcher conditions have been reported by Tewary and Jain (1982). Their theory is valid when V_j is so close to V_D that the inequality (185) is satisfied. As is apparent from Eq. (186), the theory of Tewary and Jain (1982) does explain the observation 1. However, in reality, the observation 1, i.e., the low slope region in the FCVD curve, is observed at a much lower level of injection than required by the inequality (185). As pointed out by Green (1984), this inequality is not satisfied in an ordinary diode even at an enormous current level of 10^4 A/cm^2.

On the other hand, if the Misawa voltage condition is used at the junction, it would predict that the voltage decay is faster in the beginning. This can be easily seen from Eq. (27), which is the limiting form of the Misawa condition at extreme high injections. It has been a usual practice in the literature to use Eq. (27) as the voltage condition at high injections (see, for example, Green, 1984). However, it may be remarked that Eq. (27) is also valid only in the limit of extreme high injections which would not be normally attained in practice.

In fact if Misawa and Fletcher conditions are to represent the same physical state the limiting form of Misawa conditions as given by Eq. (28) corresponds to the limiting form of Fletcher conditions for which inequality (184) is satisfied. Actually, there is an inconsistency here if we try to relate the Misawa and Fletcher conditions in terms of the terminal and junction voltage, respectively. In the open-circuit case the terminal and the junction potential should only differ by the Dember potential. The contribution of the Dember potential is relatively small even at high injections, which can be easily verified (see, for example, Dhariwal *et al.*, 1976).

On the other hand, as we see from inequality (184) and Eq. (27), the two voltages, i.e., V_j and V_a have entirely different behaviors. The discrepancy perhaps lies in the fact that the quasi-neutrality approximation upon which the whole formalism is based may not be valid at high injections. A relation between the Misawa terminal potential and the Fletcher junction potential has been given by Hauser (1971) but in this paper the quasi-neutrality approximation has also been used.

To summarize the above discussion: (1) Fletcher conditions predict a region of low slope in the FCVD curve but at extremely high injections, i.e., when $V_j \approx V_D$. (2) At similar high injections Misawa conditions would give a region of large slope viz. double that of low injections.

B. QSE Approximation for p–n Coupling at High Injections

We have seen in the previous section that p–n coupling becomes very important at high injections. In this section we shall derive the boundary condition at the injection for the diffusion equation in the base of a device that accounts for the p–n coupling in the QSE approximation. We shall assume a moderate level of high injection such that only the base is in high injection but not the emitter. As mentioned at the beginning of this section, the base reaches the high injection state at a relatively lower level of injection. The emitter is very heavily doped and would reach the state of high injection only at very high levels of injection.

By using the mass action law (see, for example, Sze, 1981) at the junction in the emitter and the base we obtain

$$(q_{e0} + q_{ej})(q_{em} + q_{ej}) = (q_{bm} + q_{bj})(q_{b0} + q_{bj}) \tag{187}$$

We assume that the emitter is in a state of low injection so that

$$q_{ej} \ll q_{em} \tag{188}$$

Also, at ordinary temperatures

$$q_{b0} \ll q_{bm} \tag{189}$$

Using the inequalities (188) and (189), the following relation can be easily derived:

$$q_{ej} = \alpha'_1 q_{bj} + \alpha'_2 q_{bj}^2 \tag{190}$$

where

$$\alpha'_1 = q_{e0}/q_{b0} \tag{191}$$

and

$$\alpha'_2 = \alpha'_1/q_{bm} \tag{192}$$

Now we invoke the QSE approximation, that the slope of the ECP in the emitter does not change during decay. First, we see by putting $X_e = 0$ in Eq. (153) that

$$f_1(z) = q_{ej}(z)/q_{ej}(z = 0) \tag{193}$$

Hence Eq. (153) can be written in the following form:

$$q_e(X_e, z) = \frac{q_e(X_e, 0)}{q_{ej}(z = 0)} q_{ej}(z) \tag{194}$$

Using Eq. (194) for $q_e(X_e, z)$ in the zero-current condition given by Eq. (154) and then Eq. (190) for $q_{ej}(z)$, we obtain the following relation:

$$\left[\frac{\partial q_b(X_b, z)}{\partial X_b}\right]_{X_b = 0} = \alpha_1 q_{bj}(z) + \alpha_2 q_{bj}^2(z) \tag{195}$$

where

$$\begin{aligned} \alpha_1 &= \frac{J_{e0}}{J_{b0}}\left[\frac{df_e(X_e)}{dX_e}\right]_{X_e = 0} \\ \alpha_2 &= \alpha_1/q_{bm} \end{aligned} \tag{196}$$

and $f_e(X_e)$ is the normalized steady-state ECP in the emitter, that is,

$$f_e(X_e) = q_e(X_e, 0)/q_{ej}(z = 0) \tag{197}$$

Equation (195) gives the desired boundary condition at the junction that accounts for p–n coupling in the QSE approximation. The parameter α_2 and the quadratic term on the right-hand side of Eq. (195) arise from the high injection effects. For $q_{bm} = \infty$, the base can not be in high injection by definition, so that $\alpha_2 = 0$. In this case, if we take the steady-state ECP to be exponential as given by Eq. (36) for a thick diode, Eq. (195) reduces to the low injection boundary condition as given by Eq. (156).

C. FCVD at High Injections

In this section we shall discuss the theory of FCVD at moderately high injections using the QSE approximation. These calculations have been carried out by Jain *et al.* (1986). We assume, as in Section VI.B, that the emitter is in a state of low injection. First we consider a thick diode, i.e., for infinite W_b and W_e. The diffusion equation for the base is as given by Eq. (125). The boundary condition at the junction is taken to be that given by Eq. (195) in the QSE approximation. For a thick emitter the steady-state ECP is given by Eq. (36) so

that, as mentioned at the end of the preceding section,

$$\alpha_1 = a \tag{198}$$

The other boundary and initial conditions are the same as taken for the base in Section IV.B viz. Eq. (127) for $q_b(X_b, z)$ and Eq. (131) as well as Eq. (37).

The solution of the diffusion equation can now be obtained by the Laplace transform method. Following the steps leading to Eq. (157), the following nonlinear Volterra integral equation for FCVD can be obtained after some algebraic manipulation:

$$\hat{q}_{bj}(z) = W_0(z) - a_1 \int_0^z \hat{q}_{bj}^2(y) K(z - y)\, dy \tag{199}$$

where

$$\hat{q}_{bj}(z) = q_{bj}(z)/q_{bj}(z = 0) \tag{200}$$

$$W_0(z) = [e^{-z} S(z) - aS(a^2 z)]/(1 - a) \tag{201}$$

$$a_1 = \alpha_2 q_{bj}(z = 0)$$

and

$$K(z) = \frac{e^{-z}}{\sqrt{\pi z}} - ae^{-z} S(a^2 z) \tag{202}$$

The ECC at the junction $q_{bj}(z)$ can be related to the junction potential by using the Fletcher voltage condition given by Eq. (23). We restrict ourselves to the case when the level of injection is not extremely high so that

$$|V_j - V_D| > kT/q \tag{203}$$

and

$$\exp[2q(V_j - V_D)/kT] \ll 1 \tag{204}$$

This is a reasonable assumption since, as mentioned in Section VI.A, in most cases of practical interest V_j does not reach close enough to V_D to violate the inequality (203). Further, even with a substantial band narrowing

$$q_{b0} > q_{e0}$$

Then, Eq. (23) reduces to the usual Shockley relation given by Eq. (29).

Thus we find that, although the base is assumed to be in high injection, q_{bj} can be assumed to obey the Shockley voltage condition. On the other hand, even if the emitter is in low injection, the Shockley condition would be a poor approximation for q_{ej} unless V_j is so small that the product $q_{b0} \exp[q(V_j - V_D)/kT]$ is negligible, which is in fact the low injection limit.

Jain *et al.* (1986) have solved Eq. (199) numerically. Their calculated FCVD for a n^+–p diode have been shown in Fig. 31 for different values of the steady-state junction voltage $V_j(0)$, which is a measure of the level of injection. For this diode $q_{bm} = 10^{13}\,cm^{-3}$, $q_{em} = 10^{20}\,cm^{-3}$, $J_{e0} = 10^{12}\,A/cm^2$, $\tau_b = 20\,\mu sec$, and $a = 0.04$. The value of a was deliberately chosen to be low, which neglects the gop shrinkage in the emitter, in order to underline the importance of p–n coupling at high injections. For such a low value of a, as discussed in Sections IV and V, the p–n coupling will be negligible at low injections.

In Fig. 31, the curve for $V_j(0) = 0.5$ is well within the low injection limit. It has the expected behavior of a low injection FCVD in a base-dominated diode. As $V_j(0)$, i.e., the injection level increases, the voltage decay in the initial stages become faster. This is obviously due to the increased p–n coupling.

The FCVD curves in Fig. 31 are shown only for $z \geq 0.1$ because the QSE approximation itself is not valid for smaller values of z. For $z \gg 1$, the nonlinear term on the right-hand side of Eq. (199) becomes negligible and FCVD is determined by the low injection term $W_0(z)$. As we have already seen in Section IV.B, it would give a linear region in the FCVD curve with unit slope. This slope, however, will only give τ_b for low injections and not the excess carrier lifetime at high injection.

Jain *et al.* (1986) have also calculated FCVD in an ideal BSF diode (SRV = 0) with finite W_b. The boundary condition at $X_b = W_b$ is given by Eq. (13) and the initial steady-state ECP is given by Eq. (46) for $S_b^* = 0$. The

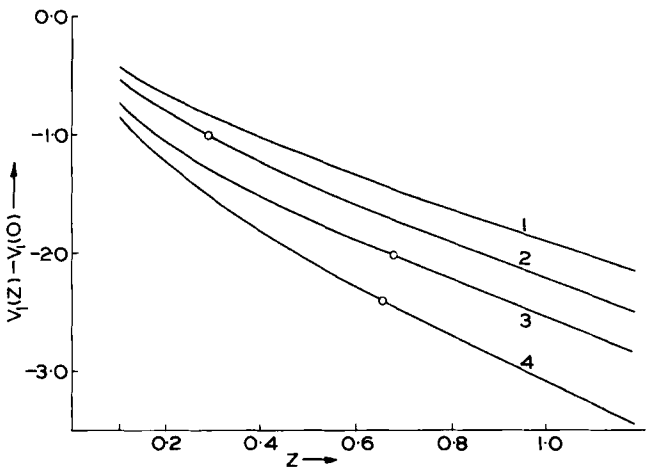

FIG. 31. $V_j(z) - V_j(0)$ is plotted as a function of z for various values of junction voltages in a thick base diode. Curves 1 to 4 are for $V_j(0) = 0.50$, 0.62, 0.64, and 0.66 V, respectively. The value of a for all the plots is taken as 0.04.

boundary condition at the junction is same as given by Eq. (195). The diffusion equation is solved by using the Laplace transform method. This leads to the following nonlinear Volterra integral equation for $q_{bj}(z)$

$$\hat{q}_{bj}(z) = K_0(z) - a\int_0^z \hat{q}_{bj}(y)K_0(z-y)\,dy - a_1\int_0^z \hat{q}_{bj}^2(y)K_2(z-y)\,dy \tag{205}$$

where

$$K_0(z) = 1 - \tanh W_b\left[\operatorname{erfc}\sqrt{z} + 2\sum_{r=1}^{\infty}\psi_1(2rW_b, z)\right] \tag{206}$$

$$K_2(z) = \frac{e^{-z}}{\sqrt{\pi z}} + \frac{2e^{-z}}{\sqrt{\pi z}}\sum_{r=1}^{\infty}\exp\left(-\frac{r^2W_b^2}{z}\right) \tag{207}$$

a_1 has been defined in Eq. (202) and ψ_1 in Eq. (99).

Equation (207) is slightly more general than that derived by Jain *et al.* (1986), who have approximated the steady-state ECP in the base to be constant. This is of course a reasonable approximation for small W_b for $S_b^* = 0$.

The calculated FCVD curves, obtained from a numerical solution of Eq. (205), for different values of W_b are shown in Fig. 32. The curves are

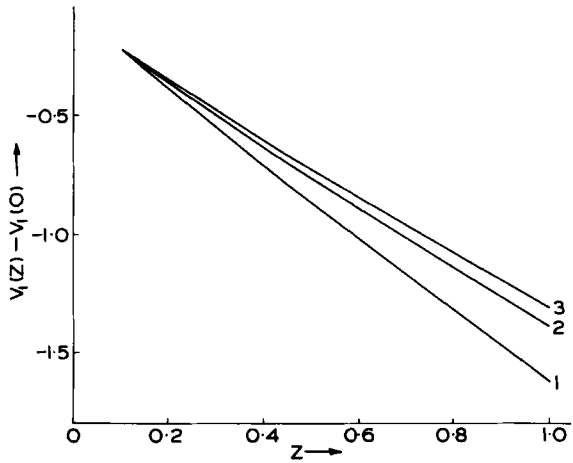

FIG. 32. $V_1(z) - V_1(0)$ is plotted as a function of z for various values of base widths in a BSF solar cell. Curves 1 to 3 are for $W_b = 0.5, 0.75$, and 1.0, respectively. The value of a is 0.01 and the initial voltage is 0.66 V for all the curves.

almost linear as expected for small W_b. The slope of these curves gives τ_{eff}, an effective value of the excess carrier lifetime as defined in Section III.C. It may be remarked that there is a slight change in slope of the FCVD curves with z but it is too small to be apparent in the figure.

We may note that the theory as given here is valid only at a moderate level of injection. It can not explain the two characteristic high injection effects, i.e., the observations 1 and 2 described at the beginning of Section IV.A. Jain *et al.* (1986) have also carried out some experimental measurements on FCVD in a BSF in an attempt for a qualitative verification of their theory.

Instead of directly comparing the theoretical and experimental FCVD curves, Jain *et al.* (1986) have compared the theoretical and experimental curves of τ_b/τ_{eff} as a function of initial voltage $V_j(0)$. These curves are shown in Fig. 33 for different values of the coupling parameter a. The experimental results are shown for two different devices with different values of a which were known from independent measurements. We see from Fig. 33 that the agreement between the calculated and the experimental curves of τ_b/τ_{eff} is quite reasonable.

D. FCVD in p–i–n Diodes

In this section we shall briefly consider FCVD in p–i–n diodes. The base of a p–i–n diode, being intrinsic by definition will be in high injection at any level of injection. In practice, the base of a p–i–n diode is not exactly intrinsic. However, the doping concentration in the base is quite small and therefore it

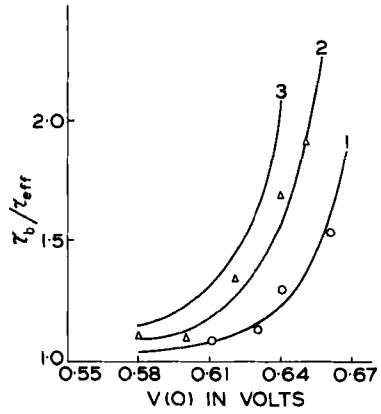

FIG. 33. The ratio τ_b/τ_{eff} is plotted as a function of the initial voltage $V(0)$. Curves 1 to 3 are the theoretical plots for $a = 0.01$, 0.02, and 0.03, respectively. The points marked by ○ and △ are the experimental results for cells A and B, respectively.

reaches the high injection state at fairly low levels of injection. It may be remarked that a BSF diode like n^+–p–p^+ would also behave like a p–i–n (or n–i–p) diode at a very high level of injection. This is because, as explained in Section II.B.2, in the limit of high injections when the ECC is much larger than the doping concentration, a doped semiconductor behaves like an intrinsic one.

The characteristic feature of a p–i–n diode is that it has two junctions, one each at the two ends of the base, i.e., p–i and i–n. The p and n regions are referred to as emitters and the i region is referred to as the base. The coupling between the emitter and the base at the two junctions will be still referred to as p–n coupling for the purpose of uniformity of nomenclature.

We assume that the injection is not high enough so that both the emitters can be assumed to be in low injection state. The boundary conditions at the two junctions, which include the effect of p–n coupling, can be obtained by using the QSE approximation as in deriving Eq. (195). These are given below.

$$\left[\frac{\partial \hat{q}_b(X_b, z)}{\partial X_b}\right]_{X_b=0} = a\hat{q}_{j1}(z) + a_1\hat{q}_{j1}^2(z) \tag{208}$$

and

$$\left[\frac{\partial \hat{q}_b(X_b, z)}{\partial X_b}\right]_{X_b=W_b} = b\hat{q}_{j2}(z) + b_1 q_{j2}^2(z) \tag{209}$$

where

$$\hat{q}_b(X_b, z) = q_b(X_b, z)/q_{j1}(z = 0) \tag{210}$$

a and a_1 are coupling parameters at the junction at $X_b = 0$, which are the same as defined in Section VI.C. The corresponding coupling parameters at the junction $X_b = W_b$ are given by b and b_1, respectively. The junctions at $X_b = 0$ and $X_b = W_b$ have been denoted by the subscripts j1 and j2, respectively.

The total junction voltage in a p–i–n diode is given by the sum of the two junction voltages, viz.

$$V_j = V_{j1} + V_{j2} \tag{211}$$

where V_{j1} and V_{j2} are obtained from q_{j1} and q_{j2}, respectively, by using the Shockley voltage condition given by Eq. (29). As mentioned in Section VI.C, even when the base is in high injection, the Shockley voltage condition is a reasonable approximation unless V_{j1} and/or V_{j2} are too close to the corresponding diffusion potential.

The diffusion equation for the base is the same as used in the earlier sections, i.e., Eq. (125). Its solution, subject to boundary conditions and the appropriate initial condition taking the steady-state ECP in a p–i–n diode,

can be formally obtained either by the Laplace transform method or by expansion in terms of eigenfunctions. However, because of nonlinear boundary conditions, one has to resort to numerical methods to obtain the final solution.

Schlangenotto and Gerlach (1972) have discussed the theory of FCVD in p–i–n diodes. In their calculations, they have taken only the quadratic terms on the right-hand side of Eqs. (208) and (209) taking $a = b = 0$, but a_1 and b_1 are taken to be nonzero. For a symmetric p–i–n diode in which $q_{j1}(z) = q_{j2}(z)$ and $a_1 = b_1$, Schlangenotto and Gerlach (1972) have derived the following nonlinear equation in terms of the variable t (not z):

$$q_{j1}(t) = q_{j1}^0(t) - a_{SG} \int_0^t \frac{e^{-(t-\lambda)/\tau_b} q_{j1}^2(\lambda)\, d\lambda}{\Delta(t-\lambda)} \tag{212}$$

where a_{SG}, the coupling parameter, is related to $a_1 = b_1$ as follows:

$$a_{SG} = a_1 L_b/\tau_b \tag{213}$$

$q_{j1}^0(t)$ is the value of $q_{j1}(t)$ in the absence of p–n coupling, that is, when $a_{SG} = 0$,

$$\Delta(t) = \frac{W_b}{\theta_3(0, i\pi t/W_b^2\tau_b)} \tag{214}$$

and θ_3 is the Jacobian function defined by

$$\theta_3(0, iz) = \frac{1}{\sqrt{z}}\left[1 + 2\sum_{r=1}^{\infty} \exp(-r^2\pi/z)\right] \tag{215}$$

for small z and the following for large z:

$$\theta_3(0, iz) = 1 + 2\sum_{r=1}^{\infty} \exp(-r^2\pi z) \tag{216}$$

Equation (212) has to be solved numerically. However, Schlangenotto and Gerlach (1972) have given the following expression which can serve as an approximate representation of the solution of Eq. (212):

$$\hat{q}_{j1}(t') = \frac{4\sqrt{t'}}{1 + 4\sqrt{t'} + \sqrt{(1 + 8\sqrt{t'})}} \tag{217}$$

where $\hat{q}_{j1}(t')$ is normalized according to Eq. (210),

$$t' = t/\tau_{SG} \tag{218}$$

and

$$\tau_{SG} = \frac{\pi L_b^2}{q_{j1}^2(t=0) a_{SG}^2 \tau_b} \tag{219}$$

The numerical solution of Eq. (212) as obtained by Schlangenotto and Gerlach (1972) agrees quite well with the approximate result obtained from Eq. (217). The main feature of the result is the rapid initial decay which is attributed to a strong p–n coupling. For example, taking $q_{j1}(t = 0) = 5 \times 10^{17}\ \text{cm}^{-3}$, $a_{SG} = 2 \times 10^{-14}\ \text{cm}^4/\text{sec}$, and $D_b(= L_b^2/\tau_b) = 6.5\ \text{cm}^2/\text{sec}$ we obtain

$$\tau_{SG} = 0.2 \quad \mu\text{sec}$$

For this value of τ_G, q_{j1} falls to half its value in only 0.2 μsec.

Equation (217) gives the decay of ECC at the junction. The result for FCVD can be simply obtained by using the Shockley voltage condition given by Eq. (29) qualitatively, the nature of the FCVD curve as obtained from these results is similar to that obtained by Jain *et al.* (1986) for a BSF diode.

E. Possible Explanation for the Occurrence of Hump in the FCVD Curve

We see that neither the theory of Jain *et al.* (1986) nor that of Schlangenotto and Gerlach (1972) explains the existence of the hump or plateau in the FCVD curve (observation 2 in Section VI.A). Both these theories give a rapid decay in the initial stages but the rise or saturation in the voltage curve are not predicted by these theories. Of course, as mentioned in Section VI.A, the experimental situation is also not quite clear.

What seems to be reasonably certain experimentally is that a hump/plateau in the FCVD curve occurs only in a two-junction device, i.e., a p–i–n or a BSF diode. The physical processes which might be responsible for causing the hump/plateau are not yet understood. We can only offer the following suggestions:

1. Dember effect—the Dember voltage depends upon the ratio of the ECC at the two junctions (see, for example, Gandhi, 1977) viz.

$$V_{Dem} \propto \ln\left(\frac{q_{b0} + q_{j1}}{q_{b0} + q_{j2}}\right) \tag{220}$$

The voltage can be assumed to be added to the junction voltage. It is tempting to try to explain the hump in the FCVD curves in terms of the change of sign V_{Dem}. As is apparent from Eq. (220), V_{Dem} can change sign if q_{j1} and q_{j2} decay at different rates, which is possible in nonsymmetric p–i–n diodes. However, a detailed examination shows that the Dember term is not large enough to compensate for the decay of the junction voltage and show a rise in the FCVD curve. Of course, Eq. (220) is based upon the quasi-neutrality approximation, which itself may not be valid at high injections.

2. Change in the strength of the p–n coupling. This would seem to be a more promising line of thought. At high injections, as we have shown in Section VI.A, the p–n coupling is quite strong. It results in a rapid decay of ECC at the junction as shown in Sections VI.C and VI.D and, of course, as physically expected. In a p–i–n or an ideal BSF diode, if the thickness of the base is much smaller as compared to the diffusion length in the base, the ECP will remain almost flat in the middle region of the device.

Since the ECC at the junction has substantially decayed due to p–n coupling but not in the middle region of the base, the gradient of the ECP near the junction will become quite large. The junction will gain carriers by diffusion from the middle region of the device. Moreover, since the ECC at the junction has decreased, the p–n coupling will become weak and therefore further loss of carriers to the emitter will become negligible.

For a suitable choice of parameters it is possible, in principle, that the diffusive gain of carriers at the junction may temporarily exceed the total loss of carriers from the junction due to recombination and the p–n coupling. It is thus possible that ECC at the junction may build up after the initial decrease. After some time the ECP will become flat near the junction. The diffusion will then become negligible and the carriers will decay again (mainly by recombination).

This process does explain, in principle, the occurrence of the hump in the FCVD curve. The plateau is a special case of the hump when the gain of carriers at the junction just equals the losses. It would be worthwhile to mathematically model this process in a theory of high injection FCVD and to attempt to explain the rather fascinating occurrence of hump/plateau in the FCVD curve.

Appendix: List of Symbols and Notations

A list of symbols/notations is given below in alphabetical order. In addition to these, some other symbols/notations have been defined locally in the text. In general the subscripts e and b refer, respectively, to the emitter and the base regions of a device (diode or solar cell).

α	Absorption coefficient of light in a solar cell
a	Coupling parameter (approximately equal to $1/j$)
$C_{e,b}$	$\alpha L_{e,b}$
$D_{e,b}$	Diffusion coefficient for minority carriers
$D_{em,bm}$	Diffusion coefficient for majority carriers
$d_{e,b}$	Thickness of emitter (e)/base (b)

$E_{e,b}$	Drift field
$E_{ej,bj}$	Drift field at the junction
ECC	Excess carrier concentration
ECP	Excess carrier profile
η	Surface generation coefficient
$F_{e,b}$	Drift field in dimensionless units ($=qE_{e,b}L_{e,b}/2kT$)
$g_{e,b}$	Generation rate of excess carriers
$J_{ej,bj}$	Current at the junction
J_j	Total junction current ($J_{bj} + J_{ej}$)
$J_{e0,b0}$	Thermal equilibrium saturation current
J_0	Total thermal equilibrium saturation current ($J_{e0} + J_{b0}$)
j	Ratio of saturation currents ($=J_{b0}/J_{e0}$)
kT/q	Boltzmann voltage factor
$L_{e,b}$	Diffusion length for minority carriers
$\mu_{e,b}$	Mobility of minority carriers
N_0	Number of photons incident per second per unit area at the front surface in a solar cell
N_{0j}	Number of protons incident per second per unit area at the junction in a solar cell
$q_{e,b}$	ECC
$q_{ej,bj}$	ECC at the junction
$q_{e0,b0}$	Minority carrier concentration at thermal equilibrium
q_{es}	ECC in the steady state
$q_{em,bm}$	Majority carrier concentration at thermal equilibrium (doping concentration)
q_i	Intrinsic carrier concentration
R_s	Series resistance of diode/solar cell
SRV	Surface recombination velocity
$S_{e,b}$	SRV
$S^*_{e,b}$	Dimensionless SRV ($=S_{e,b}\tau_{e,b}/L_{e,b}$)
ξ	Ratio of lifetimes ($=\tau_b/\tau_e$)
t	Time variable
$\tau^*_{e,b}$	Excess carrier lifetime (ambipolar)
$\tau_{e,b}$	Minority carrier lifetime
$\tau_{e0,b0}$	Minority carrier lifetime at thermal equilibrium
$\tau_{em,bm}$	Majority carrier lifetime
$\tau_{em0,bm0}$	Majority carrier lifetime at thermal equilibrium
V_a	Terminal potential across diode/solar cell
V_D	Diffusion (built-in) potential
V_j	Junction potential
V_i	Dimensionless junction potential ($=qV_j/kT$)
x	Distance variable

$X_{e,b}$ Dimensionless distance variable ($=x/L_{e,b}$)
Z Dimensionless time variable (t/τ_b)

REFERENCES

Abramowitz, M., and Stegun, I. E., eds. (1965). "Handbook of Mathematical Functions." Douer, New York.

Agarwala, A., and Tewary, V. K. (1980). *J. Phys. D* **13,** 1885.

Agarwala, A., Tewary, V. K., Agarwal, S. K., and Jain, S. C. (1980). *Solid-State Electron.* **23,** 1021.

Backus, C. E., ed. (1976). "Solar Cells." Inst. Electr. Electron. Eng., New York.

Baliga, B. (1981). *In* "Silicon Integrated Circuits" (D. Kahng, ed.), Appl. Solid State Sci. Suppl. 2, Part B, p. 109, Academic Press, New York.

Bassett, R. J., Fulop, W., and Hugarth, C. H. (1973). *Int J. Electron.* **35,** 177.

Carslaw, H. S., and Jaeger, J. C. (1959). "Conduction of Heat in Solids," 2nd ed. Oxford Univ. Press, London and New York.

Cooper, R. W. (1983). *Solid-State Electron.* **26,** 217.

Derdouri, M., Letureq, P., and Munoz-Yague, A. (1980). *IEEE Trans. Electron Devices* **ED-27,** 2097.

Dhariwal, S. R., and Vasu, N. K. (1981). *IEEE Electron Device Lett.* **EDL-2,** 53.

Dhariwal, S. R., Kothari, L. S., and Jain, S. C. (1976). *IEEE Trans. Electron Devices* **ED-23,** 504.

Dhariwal, S. R. Kothari, L. S., and Jain, S. C. (1981). *Solid-State Electron.* **24,** 749.

Fahrenbuch, A. L., and Bube, R. H. (1983). "Fundamentals of Solar Cells." Academic Press, New York.

Fletcher, N. H. (1957). *Int. J. Electron.* **2,** 609.

Fossum, J. G., Lindholm, F. A., and Shibib, M. A. (1979). *IEEE Trans. Electron Devices* **ED-26,** 1294.

Gandhi, S. K. (1977). "Semiconductor Power Devices." Wiley, New York.

Gossick, B. R. (1955). *J. Appl. Phys.* **26,** 1356.

Green, M. A. (1984). *Sol. Cells* **11,** 147.

Guckel, H., Thomas, B. C., Iyengar, S. V., and Demirkol, A. (1977). *Solid-State Electron.* **20,** 647.

Hauser, J. R. (1971). *Solid-State Electron.* **14,** 133.

Heasell, E. L. (1979). *Solid-State Electron.* **22,** 853.

Hovel, H. J. (1975). *In* "Semiconductors and Semimetals," (R. K. Willardson and A. C. Beer, eds.), Vol. 11. Academic Press, New York.

Jain, S. C. (1981). *Solid-State Electron.* **24,** 179.

Jain, S. C., and Muralidharan, R. (1981). *Solid-State Electron.* **24,** 1147.

Jain, S. C., and Ray, U. C. (1983a). *Solid-State Electron.* **26,** 515.

Jain, S. C., and Ray, U. C. (1983b). *J. Appl. Phys.* **54,** 2079.

Jain, S. C., Ray, U. C., Muralidharan, R., and Tewary, V. K. (1986). *Solid-State Electron.* **29,** 561.

Joshi, S. C., and Singhal, C. M. (1982). *Int. J. Electron.* **52,** 381.

Kennedy, D. P. (1962). *IRE Trans. Electron Devices* **ED-9,** 174.

Kingston, R. H. (1954). *Proc. IRE* **42,** 829.

Lederhandler, S. R., and Giacoletto, L. J. (1955). *Proc. IRE* **43,** 477.

Lindholm, F. A., and Sah, C. T. (1976). *J. Appl. Phys.* **47,** 4208.

McKelvey, J. P. (1966). "Solid State and Semiconductor Physics." Harper & Row, New York.

Madan, M. K., and Tewary, V. K. (1983). *Sol. Cells* **9,** 289.

Madan, M. K., and Tewary, V. K. (1985). *Ind. J. Pure Appl. Phys.* (in press).
Mahan, J. E., Ekstedt, T. W, Frank, R. I., and Kaplow, R. (1979). *IEEE Trans. Electron Devices* **ED-26,** 733.
Mallenson, J. R., and Landsberg, P. T. (1977). *Proc. R. Soc. Ser. London, A* **355,** 115.
Misawa, T. (1956). *J. Phys. Soc. Jpn.* **11,** 728.
Moll, J. L. (1964). "Physics of Semiconductors." McGraw-Hill, New York.
Moore, A. R. (1980). *RCA Rev.* **40,** 549.
Muralidharan, R., Jain. S. C., and Jain, V. (1982). *Sol. Cells* **6,** 157.
Neville, R. C. (1980). "Solar Energy Conversion: The Solar Cells." Am. Elsevier, New York.
Nosov, Y. R. (1969). "Switching in Semiconductor Diodes." Plenum, New York.
Nussbaum, A. (1969). *Solid-State Electron.* **12,** 177.
Nussbaum, A. (1975). *Solid-State Electron.* **18,** 107.
Nussbaum, A. (1979). *Solid-State Electron.* **21,** 1178.
Ray, U. C., Agarwal, S. K., and Jain, S. C. (1982). *J. Appl. Phys.* **53,** 9122.
Rose, B. H. (1981). *IEEE Int. Electron Devices Meet. 1981.*
Sah, C. T., Noyce, R. N., and Shockley, W. (1957). *Proc. IRE* **45,** 1228.
Scharfetter, D. L., Lade, R. W., and Jordon, A. G. (1963). *IEEE Trans. Electron Devices* **ED-10,** 35.
Schlangenotto, H., and Gerlach, W. (1972). *Solid-State Electron.* **15,** 393.
Sharma, S. K., and Tewary, V. K. (1982). *J. Phys. D* **15,** 1077.
Sharma, S. K., and Tewary, V. K. (1983). *J. Phys. D* **16,** 1741.
Sharma, S. K., Agarwala, A., and Tewary, V. K. (1981). *J. Phys. D* **14,** 1115.
Shockley, W. (1950). "Electrons and Holes in Semiconductors." Van Nostrand-Reinhold, Princeton, New Jersey.
Sneddon, I. N. (1972). "The Use of Integral Transforms." McGraw-Hill, New York.
Sze, S. M. (1981). "Physics of Semiconductor Devices," 2nd ed. Wiley, New York.
Tewary, V. K., and Jain, S. C. (1980). *J. Phys. D* **13,** 835.
Tewary, V. K., and Jain, S. C. (1982). *Solid-State Electron.* **25,** 903.
Tewary, V. K., and Jain, S. C. (1983). *Ind. J. Pure Appl. Phys.* **21,** 36.
Van der Ziel, A. (1966). *Solid-State Electron.* **16,** 1509.
Van Vliet, K. M. (1966). *Solid-State Electron.* **9,** 185.
Weaver, H. T. (1981). *Int. Workshop Phys. Solid State Devices, 1981.*
Wolf, M. (1963). *Proc. IEEE* **51,** 674.